AE-445
UDC 539.171.017:
539.171.4
546.293-14

AE-445

Neutron Inelastic Scattering Study of Liquid Argon

K. Sköld, J. M. Rowe,
G. Ostrowski and P. D. Randolph

AKTIEBOLAGET ATOMENERGI
STUDSVIK, NYKÖPING, SWEDEN 1972

NEUTRON INELASTIC SCATTERING STUDY OF LIQUID ARGON*

by

K Sköld**, J M Rowe, G Ostrowski
Solid State Science Division, Argonne National Laboratory,
Argonne, Illinois, USA

and

P D Randolph
Nuclear Technology Division, Idaho Nuclear Corporation,
Idaho Falls, Idaho, USA***

ABSTRACT

The inelastic scattering functions for liquid argon have been measured at 85.2 K. The coherent scattering function was obtained from a measurement on pure A-36 and the incoherent function was derived from the result obtained from the A-36 sample and the result obtained from a mixture of A-36 and A-40 for which the scattering is predominantly incoherent. The data, which are presented as smooth scattering functions at constant values of the wave vector transfer in the range 1.0 - 4.4 $Å^{-1}$, are corrected for multiple scattering contributions and for resolution effects. Such corrections are shown to be essential in the derivation of reliable scattering functions from neutron scattering data. The incoherent data are compared to recent molecular dynamics results and the mean square displacement as a function of time is derived. The coherent data are compared to molecular dynamics results and also, briefly, to some recent theoretical models.

---

* Based on work performed under the auspices of the U S Atomic Energy Commission. Part of this work was performed under a grant from the Swedish National Research Council

** On leave from AB Atomenergi, Studsvik, Sweden, now returned

*** Now at Aerojet Nuclear Co, Idaho Falls, Idaho, USA

Printed and distributed in February 1972

CONTENTS

I. INTRODUCTION

Although a considerable amount of insight into the dynamical behaviour of atoms in liquids has been gained during recent years through the results obtained from inelastic neutron scattering experiments, earlier studies have been of limited utility because of various experimental uncertainties - most importantly, the effects of multiple scattering. The present report attempts to correct these deficiencies for liquid argon, and we describe in detail the data analysis leading to the corrected scattering laws presented. In spite of some remaining problems (principally connected with estimation of errors in the final results), we believe that the present results are sufficiently reliable to allow quantitative comparisons with both theory and molecular dynamics results. An important feature of the present results is that the absolute normalization of the scattering functions has been obtained experimentally.

The theoretical description of the complex many-body problem which the liquid constitutes is conveniently made in terms of two functions. One of these is concerned only with the average motion of one atom among the other atoms (Van-Hove self-correlation function) while the other function describes the relative motion of atoms (density correlation function). In principle the neutron scattering experiments allow a complete determination of both of these functions. In practice, however, competing requirements on intensity and resolution and systematic errors such as multiple scattering contamination limit the amount and reliability of the information that is obtained. The information about the density correlation function is contained in the coherent scattering function while the Van-Hove self-correlation function is obtained from the incoherent scattering. In general the scattering properties of a sample are such that a combination of both the coherent and incoherent scattering function is observed in the neutron scattering experiment. The theoretical efforts, on the other hand, are concerned either exclusively with the density correlation function or exclusively with the self-correlation function even though, in principle, both functions should follow from a complete theoretical description of the liquid state. In order to facilitate comparison between experimental results and specific theoretical predictions it is therefore important that the scattering laws be obtained separately. Also, in several

recent models the density correlation function is obtained in terms of the self-correlation function and the equilibrium pair distribution function [1-7]. In order to test these models against experimental results for the coherent scattering function, it is important that the incoherent function, which is used as input in the theory, be determined separately.

A large amount of theoretical work has been done during recent years both on the self motion [18-26] and on the correlated motion of atoms in liquids [1-17]. The theoretical studies have so far dealt almost exclusively with monatomic systems. In the case of the self-correlation function there are no neutron scattering results available at all for simple monatomic liquids. The only elements with almost totally incoherent scattering are hydrogen and vanadium. Due to the high melting point and the difficulties in finding a suitable container material, liquid vanadium has not yet been studied. Hydrogen, on the other hand, forms a molecular system which considerably complicates the theoretical analysis. The only data available so far for the self-correlation function in monatomic liquids are the molecular dynamics results of Rahman [7] and of Levesque and Verlet [27].

Several liquid metals with predominantly coherent scattering have been studied [28-31] and the results have been analysed in terms of simple theoretical models. The main result obtained so far is that collective excitations with a wave vector dependence resembling that observed in solids seem to exist in the liquid metal. Rather similar conclusions were drawn from neutron scattering results for liquid argon [32, 33]. However, as the samples had the natural abundance of argon isotopes, the observed scattering was a mixture of incoherent and coherent scattering and, as mentioned above, this makes the analysis of the results less straightforward. With the increased theoretical efforts and the lack of experimental results in this area in mind the present experiment, in which the separated incoherent and coherent scattering laws for liquid argon at 85.2 K were obtained, was undertaken.

The coherent scattering law was obtained directly from a measurement on A-36 for which the scattering is purely coherent. There is no composition of argon isotopes for which the scattering is purely incoherent. The incoherent scattering law was in the present experiment derived from the scattering data obtained from a mixture of A-36 and A-40 with the composition adjusted so that the ratio of incoherent

to coherent scattering was close to the maximum value possible ($\sigma_{inc}/\sigma_{coh} = 2.9$). The coherent scattering contribution to the mixture data was removed by subtracting the properly normalized results obtained for the coherent scattering from the A-36 sample.

Much effort has been devoted to the correction of the data for contamination by mulitply scattered neutrons. This contamination is especially serious in the case of the coherent scattering law for small values of the wave vector transfer, where the primary intensity is low. The data have also been corrected for energy resolution broadening. This correction is of major importance for the incoherent data at small values of the wave vector transfer, and is also of importance for the coherent scattering law at values of the wave vector transfer in the region of the first peak in the structure factor.

This report is concerned mainly with the presentation of the experimental results and the description of the various procedures employed in deriving smooth scattering functions at fixed values of the wave vector transfer from the raw data obtained in the scattering experiment. The results are compared to the molecular dynamics results by Levesque and Verlet [27] in the case of the incoherent data and to the molecular dynamics results by Rahman [34] in the case of the coherent data. To keep the size of the report within reasonable limits, only a limited comparison with theoretical results is made. A more complete discussion of the theoretical interpretation of the present results will be given in a forthcoming paper.

The basic formulas relating the neutron scattering cross-sections to the correlation functions for the target atoms and some general properties of the scattering functions are summarized in Section II. The spectrometer, the sample arrangement and the procedure used to obtain absolute normalization of the data are described in Section III. The raw data and the double differential scattering cross-section at constant angle are presented in Section IV and the correction for multiple scattering is described in Section V. The separation of the incoherent scattering from the mixture data and the correction of the data from the almost pure A-36 sample for the incoherent contribution is described in Section VI. Details of the resolution correction are given in Section VII. The representation at constant value of the wave vector transfer of the data originally obtained at constant angle is described in Section VIII, where also the final smooth scattering functions are

presented. In Section IX, we discuss the incoherent scattering function and compare it with molecular dynamics results. Similarly, we discuss the coherent data and (briefly) some current theoretical results in Section X. Section XI, finally, comprises a summary of the major results.

II. BASIC FORMULAS

The double differential scattering cross-section which, after some trivial corrections, is obtained directly in the neutron scattering experiment is related to the sample dynamics via:

$$\frac{d^2\sigma}{d\Omega dE} = \frac{\sigma}{4\pi} \cdot \left(\frac{E+E_o}{E_o}\right)^{1/2} \cdot S(Q, E) \qquad (1)$$

where E_o is the initial energy of the neutron and E is the energy transferred to the neutron in the scattering process. Q is the wave vector transfer and S(Q, E), the scattering function, is the double Fourier-transform of the Van-Hove space-time correlation function.

For convenience we will often use a symmetric form for the scattering function:

$$\tilde{S}(Q, E) = \exp(E/2kT) \cdot S(Q, E) \qquad (2)$$

The zeroth and first energy moment of the scattering functions are known exactly, and are therefore very useful for testing the reliability of the experimental results. The second energy moment is known exactly for a classical system with velocity independent forces, and the first quantum correction, which can be estimated, is small for liquid argon in the region of interest. With the n^{th} energy moment defined as:

$$\langle E^n \rangle = \int_{-\infty}^{\infty} E^n \cdot S(Q, E)dE \qquad (3)$$

the three first moments are given by:

$$
\begin{aligned}
&\langle E^0\rangle_{INC} = 1 \\
&\langle E^0\rangle_{COH} = S(Q) \\
&\langle E^1\rangle_{INC} = \langle E^1\rangle_{COH} = \frac{\hbar^2 Q^2}{2M} \\
&\langle E^2\rangle_{INC} = \langle E^2\rangle_{COH} = \frac{\hbar^2 Q^2 kT}{M}
\end{aligned}
\tag{4}
$$

where $S(Q)$, the structure factor, is the Fourier-transform of the pair correlation function and $\langle E^2\rangle$ is the classical result.

The intermediate scattering function $F_S(Q,t)$ is obtained from the scattering function via a Fourier-transform in energy:

$$
F_S(Q,t) = 2\int_0^\infty \cos\frac{E\cdot t}{\hbar}\cdot \mathfrak{S}_{INC}(Q,E)dE \tag{5}
$$

As shown by Nijboer and Rahman [35], the intermediate scattering function is conveniently expressed as a Gaussian in Q multiplied by a factor that describes the non-Gaussian behaviour:

$$
F_S(Q,t) = e^{-\frac{\hbar^2 Q^2}{8Mk_BT}}\cdot e^{-Q^2\cdot\rho(t)}\cdot\left[1+\alpha_2(t)\cdot\frac{(Q^2\cdot\rho(t))^2}{2}+\ldots\right] \tag{6}
$$

The first factor on the right hand side is a consequence of the use of the symmetric form for the scattering function. From the analysis of molecular dynamics results Nijboer and Rahman conclude that it is sufficient to include the first correction term in the expansion above. In this approximation $F_S(Q,t)$ is thus specified by the width function $\rho(t)$ and the coefficient $\alpha_2(t)$ which is defined by:

$$
\alpha_2(t) = \frac{\langle r^4\rangle}{3\langle r^2\rangle^2} - 1 \tag{7}
$$

where $\langle r^n\rangle$ is the n^{th} r-moment of the Van-Hove self-correlation function $G_S(r,t)$. As seen from Eq (7), for a Gaussian $G_S(r,t)$ the coefficient $\alpha_2(t)$ is zero. It should be noted, however, that the convergence of the series in Eq (6) is not assured for all values of Q.

III. EXPERIMENTAL DETAILS

A. Spectrometer

The experiment was performed at the phased-chopper velocity selector spectrometer at the MTR reactor at Idaho Falls. A detailed description of the instrument is given in Reference 28 and we will review the most important features only. The detectors, arranged in 15 independent groups between 18.4^{o} and 94^{o} with 1 to 3 detectors in each group, were 1 inch diameter 18 inch active length He^{3} counters. The number of detectors in a group was chosen in accordance with the requirements on angular resolution in the case of the coherent sample (compare Fig 1). As the data obtained from the A-36 were to be used as a correction for the coherent contribution to the scattering from the mixture sample, the same detector configuration, and thus the same angular resolution, was used in both cases. The flight path from sample to detector was 2.25 meters. To avoid scattering of the direct beam in the air immediately before and after the sample and scattering of the deflected beam between sample and detector the helium filled flight path described in Reference 28 was used. For the monitoring of the incident beam flux and for the determination of the incident energy distribution, three flat fission counters were placed in the beam. One of the counters was placed before the sample and could therefore, together with the two counters placed after the sample, be used to monitor the transmission of the sample. Great care was taken to shield off illuminated construction material in the sample area so that it should not be seen by the detectors. As seen below, Bragg-scattering from the aluminium in the vacuum jacket around the sample did, nevertheless, contaminate the beam in some cases.

For each of the two samples data were collected at two incident energies, E_o = 15.03 meV and E_o = 19.97 meV. Due to irregular behaviour of the beam monitors the data for E_o = 15.03 meV could not be used in the case of the mixture sample. The ranges of energy and wave vector transfer covered in the present experiment are shown in Fig 1, together with the resolution in energy and wave vector transfer for elastic scattering. The resolution functions shown in Fig 1 include the effects of an average over 5 consecutive time channels described in Section IV. Both the energy and wave vector resolution increase monotonically with energy transfer.

B. Sample arrangement

The mixture sample was contained in an aluminium tube wrapped back and forth to make up a vertical plane slab. The axis of the tube was parallel to the horizontal scattering plane over the beam area, with cadmium plates inserted between adjacent tubes in order to eliminate scattering between tubes. The inner diameter of the tube was 0.58 cm, the wall thickness was 0.0254 cm and the distance between tube centerlines was 0.67 cm.

For the A-36 sample an aluminium tube with nominal I.D. = = 0.046 cm was used. Due to the small dimension of the tube it was not possible in this case to insert neutron absorbers between adjacent tubes. In order to obtain absolute values for the scattering functions it is necessary to know the sample volume accurately, i.e. the tube dimensions must be accurately known. In the case of the narrow tube used for the A-36 sample a direct mechanical measurement of the I.D. is rather difficult. The I.D. of the tube was in this case obtained by condensing $B^{10}F_3$ in the sample container and measuring the transmission of neutrons through the sample. The transmission was measured to be 40.5 per cent. From the known absorption cross-section and number density of B^{10} and assuming that the tubes were ideal cylinders it was then possible to derive a value for the tube diameter. The value obtained was 0.055 cm. For comparison, two tubes from the same batch were calibrated by measuring the outer diameter, the length and the weight. For these tubes the value obtained for I.D. was 0.056 cm and 0.053 cm, respectively.

In the case of both samples the beam was masked off by cadmium immediately before the sample. The size of the mask was such that only the straight horizontal portions of the tubes were illuminated. This was done in order to ensure a homogeneous distribution of sample over the beam area and also to make possible the calculation of the number of atoms per unit area from the known dimension of the tube. In both cases the measurements were done in transmission with the sample at 45° angle to the incident beam direction.

The sample was kept at constant temperature in a liquid nitrogen cryostat. The temperature was determined by a NBS-calibrated platinum resistor included in the copper block to which the sample container was attached. The platinum resistor also served as sensing element in the electronic temperature control device. The temperature was 85.2 ± 0.1 K for both of the samples measured.

C. Sample data

Both of the sample gases were obtained from Mound Laboratory, Monsanto Research Corporation. The composition (in mol.-%) of the samples and the bound scattering cross-sections for the isotopes as obtained by Krohn and Ringo [48] are shown in Table 1.

Table I

	"A-36" sample	Mixture sample	σ_s(barn)
A-36	98.535	7.128	77.8±0.4
A-38	0.815	0.099	1.6±1.6
A-40	0.080	91.773	0.419±0.003
N_2	0.550	0.300	
O_2	0.010	-	
CO_2	0.010	-	
H_2	-	0.600	
H_2O	-	0.100	

From these values for the abundance and the cross-sections for the isotopes the cross-sections for the two samples are as given in Tabel II.

Table II

	"A-36" sample	Mixture sample
σ_{COH}	76.6±0.5	1.64±0.01
σ_{INC}	0.54±0.08	4.76±0.07

In computing the cross-sections shown in Table II the effect of the chemical impurities has not been included.

It will be seen below that the uncertainty in σ_{INC} for the A-36 sample gives rise to large uncertainties in $S_{COH}(Q, E)$ at small values of Q and E and, in this case, we should also take the chemical impurities into account. An accurate evaluation of the effects of the chemical impurities would, however, require precise information about the quantity of each impurity which is actually dissolved in the sample container. The scattering functions for the impurities should also be known. A rough estimate of the effect of an impurity is obtained if it is assumed that the impurity is completely dissolved in the sample liquid and that the scattering function for the impurity is the same as

for the argon isotopes. In the case of the A-36 sample, where only the nitrogen need to be considered, this would lower σ_{INC} by ~0.1 b and σ_{COH} by ~0.2 b. The maximum overall effect of the nitrogen impurity on the cross-sections is thus of the same magnitude as the error obtained from the uncertainties in the cross-sections for the individual isotopes.

D. Calibration of spectrometer constants

The relation between the measured time-of-flight distribution and the double differential scattering cross-section (barns/usec/steradian/atom) is:

$$\frac{d^2\sigma}{d\Omega dt} = \frac{N_{ij}}{E_j} \cdot \frac{E_M}{N_M^s} \cdot \frac{NF}{N_T} \cdot 10^{24} \cdot \frac{FF_i}{\Delta\Omega_i \cdot \Delta t} \qquad (8)$$

$N_{ij} = N_{ij}^s - N_{ij}^o \cdot \frac{N_M^s}{N_M^o} - FBG_j$

N_{ij}^s = counts in time channel j at angle i with sample in

N_{ij}^o = counts in time channel j at angle i with container empty

N_M^s, $N^o{}_M$ = monitor counts in sample run and in open run, respectively

FBG_j = residual time-independent intensity obtained by averaging over channels at small flight times where the true spectrum has a negligible intensity

E_M = monitor efficiency at the incident energy

E_j = detector efficiency in time channel j

NF = sample transmission. This factor corrects for the shielding of the downstream monitor by the sample

N_T = number of target atoms per cm^2

FF_i = figure of merit for the i^{th} detector channel

$\Delta\Omega_i$ = solid angle subtended by the i^{th} detector

Δt = width of time channel

In order to obtain accurate absolute values for the cross-section the spectrometer functions E_M, E_j, FF_i, $\Delta\Omega_i$ and Δt must be calibrated. In the present case this was done by determining the elastic scattering from vanadium which is given by:

$$\left(\frac{d\sigma}{d\Omega}\right)_{elastic} = \frac{\sigma_s}{4\pi} \cdot \exp(-aQ^2) \qquad (9)$$

where σ_s, the scattering cross-section, is 5.13 barns and a, the temperature factor, is 0.00677 $Å^2$. After correcting N_{ij}^s for absorption in the sample $d^2\sigma/d\Omega dt$ for vanadium was determined from Eq (8) with nominal values given to the spectrometer constants. The result was then integrated over the elastic peak and compared to Eq (9) for each angle separately. In this way new values for FF_i were determined such that the experimental and theoretical results for the elastic scattering from vanadium agreed. This value was subsequently used in the evaluation of the argon data. For the relative energy dependence of E_j a table corresponding to the nominal counter characteristics was used.

The correction for self shielding in the sample was obtained by computing the average "effective" scattering per unit volume. The "effective" scattering for a volume element is defined as the product of the primary scattering in the volume element multiplied by the probability that a neutron scattered in the direction of a detector will escape from the sample without suffering a second scattering. The data were multiplied by the ratio of the macroscopic scattering cross-section per unit volume and the average "effective" scattering cross-section per unit volume. The influence on the data of neutrons scattered several times will be considered in Section V.

IV. PRESENTATION OF DATA

Fig 2 shows the raw data for 7 out of the total of 15 angles measured in each run. In the case of the mixture sample inconsistent behaviour of the beam monitors made it necessary to discard the data obtained at E_o = 15 meV. Also shown in Fig 2 are the data obtained for the empty sample container. Bragg-scattering from the container material is evident in the case of A-36 for E_o = 15 meV and $\theta = 69.06^o$. Due to the large uncertainties resulting from the subtraction of two large and nearly equal numbers, both affected by statistics, the data in the region of a Bragg-peak were replaced by a smooth curve fitted to the data on either side of the peak.

The double differential scattering cross-section is shown in Fig 3 for the same angles for which the raw data were shown in Fig 2. The data in Fig 3 were obtained from Eq (1) as described above and converted to wave length scale. Before entering the open counts into Eq (1) a

correction was applied for the shielding by the sample of the scattering from the container material. This correction was obtained by assuming that the scattering properties of the container material are homogeneous over the tube and that a neutron scattered in the sample either after being scattered in the first wall of the tube or before reaching the point of scatter in the second wall does not contribute to the open count. This approach underestimates the total amount of container scattering present in the sample data but gives a nearly correct estimate of the influence on the data of the sharp elastic peak in the container scattering. Also shown in Fig 3 are the resolution functions at each angle as obtained from scattering from vanadium. As can be appreciated from Fig 3, the resolution broadening will seriously distort the data at the smallest scattering angles in the case of the mixture data. Resolution effects will also be rather severe for the A-36 data in the angular region where the elastic scattering occurs at wave vectors close to the first peak in the structure factor.

As the next step in the data handling the double differential cross-sections at constant angle were converted from wave-length to energy scale and then interpolated at equidistant points in energy. The interpolation was done in steps of 0.2 meV which corresponds roughly to the resolution width. For each of these energies a parabola was fitted by least squares to the 5 original data points that were closest to the selected energy. The value for $d^2\sigma/d\Omega dE$ at the desired energy was then obtained from the value of the parabola at this point.

V. MULTIPLE SCATTERING CORRECTION

In the derivation of absolute scattering functions from the results of neutron scattering, it is essential to correct the data for the effects of neutrons scattered more than once by the sample. This problem has long been recognized (although few realistic corrections have been attempted) and several authors [36-40] have proposed methods of calculation and used these to estimate such effects for various geometries. Experimentally, the problem has been attacked in several ways, the principal ones being to use samples of high transmission (>90 percent), and to use absorbing spacers [41] to further limit the scattering in the plane of the sample. As Slaggie [38] has shown, for geometries which allow adequate primary intensity, such procedures reduce, but do not remove the problem. Thus, although our samples were of high transmission (and in the mixture case had absorbing separators), we have calculated the multiple scattering corrections to our data. At

the time of this work the results of Bischoff [40], who applied generalized Monte Carlo methods to the problem, were not available, and we followed the same general procedure used by authors [36-39], adapted to our geometry.

The general procedure used was to solve the transport equations for once and twice scattered neutrons by dividing the sample volume into cells for first scattering, and then dividing the first scattered neutrons into a grid of angles (both polar and azimuthal). The total probability of second scattering of these neutrons was computed from the geometry of the sample for each point on the angular grid. The scattering probabilities were calculated using the total scattering cross-section of each sample. In the case of the A-36 sample, proper account was taken of second scattering events which occurred in neighbouring tubes. Tests of the program showed the need to include ten such tubes. Various tests were also run to check the adequacy of the cell size used for first scattering. This procedure yielded a table of numbers for the total second scattering due to a first scattering through a given pair of angles. At this point it was necessary to insert a model or kernel for singly scattered neutrons. As this kernel is precisely what we wish to measure, this presents the most serious difficulty in doing multiple scattering calculations. We tested two different models for the coherent scattering law, one due to Ailawadi et al. [12] and the other to Pathak and Singwi [9]. These two models have quite different functional forms, but both satisfy the zeroth, second and fourth moments for our sample. Comparison of the results showed little sensitivity to the models and so we used the Pathak-Singwi model, which has somewhat better characteristics at large Q and E. For the incoherent kernel, we used a simple diffusion model. This is certainly not valid at large values of Q and E but as shown later, it is a reasonable representation of the data, as the peak height and width predicted agree with our results to within about 20 per cent over the range measured. The use of this kernel is certainly the largest source of error in the calculations for the mixture sample. Having chosen kernels, we used these kernels to calculate the second scattering at each detector for both samples at 20 meV incident energy and for the coherent A-36 sample at 15 meV incident energy. (For the mixture sample we used a properly weighted sum of the two kernels.)

To estimate third scattering, we assumed that the flux of second scattered neutrons was isotropic, and then calculated third scattering

at each detector. The assumption of isotropic second scattering was justified by the fact that the calculated second scattering only varied by 20 per cent over the entire angular range. As third scattering was only 10 per cent of second scattering we did not estimate higher order scattering events. Representative plots of the multiple scattering contribution are shown together with the uncorrected data in Fig 4.

After the second and third scattering were estimated for each run, they were subtracted from the measured scattering to obtain the corrected double differential scattering cross-sections. These corrected cross-sections were then used to extract the scattering functions at constant Q as described below. From these constant Q scattering functions we were able to derive the zeroth, first and second energy moments, which were then compared to theory. The resultant improvement in the moments can be seen from Fig 10, where we show the moments for both scattering functions divided by the theoretical moments before and after the correction. The results are very gratifying, and we feel that they show both the accuracy of the present correction and the absolute necessity for such corrections. The zeroth "theoretical" moment used for the coherent case was the structure factor measured by Yarnell et al. [42] which is corrected for multiple scattering and then normalized to the accurately known values at small and large Q. The present result for S(Q), with and without the multiple scattering correction applied, is shown in Fig 5 together with the result obtained by Yarnell et al. As both our experimental data and our multiple scattering correction were derived in absolute terms, with no adjustable constants, we feel that the agreement, particularly at small Q, is most impressive.

As a final word on this topic, we would like to stress that the work of Bischoff [40], which is based upon Monte Carlo methods, is clearly the most flexible and useful approach to calculation of multiple scattering. It is relatively easy to extend the programs to other geometries, and to include the effects of container scattering when this is large (as it is when measuring liquid metals with high boiling points for example). It may well prove possible to use this program in an iterative scheme to eliminate the problem of choosing kernels, although the computation time required is not unsubstantial. In spite of this, however, we feel that the present computation is adequate to within the statistical accuracy of the data, with the major source of error

being the choice of kernels, especially in the incoherent case.

VI. SEPARATION OF SCATTERING FUNCTIONS

The scattering functions at constant angle are obtained from the double differential scattering cross-sections via Eq (1). The appropriate scattering functions for the two samples are:

$$S^{36}(Q,E) = \frac{1}{(a_c^{36})^2+(a_i^{36})^2} \cdot [(a_c^{36})^2 \cdot S_{COH}(Q,E) + (a_i^{36})^2 \cdot S_{INC}(Q,E)] \quad (9')$$

$$S^{m}(Q,E) = \frac{1}{(a_c^{m})^2+(a_i^{m})^2} \cdot [(a_c^{m})^2 \cdot S_{COH}(Q,E) + (a_i^{m})^2 \cdot S_{INC}(Q,E)] \quad (9'')$$

where the superscripts refer to the almost pure A-36 and the mixture sample respectively. Eq (9') is solved for $S_{COH}(Q,E)$ which is substituted in Eq (9''). From Eq (9'') we then obtain $S_{INC}(Q,E)$ in terms of the observed scattering functions $S^{36}(Q,E)$ and $S^{m}(Q,E)$ and the scattering lengths for the two samples which are given in Section III. In the derivation of $S_{INC}(Q,E)$ from the mixture data only the results from the A-36 sample for E_o = 20 meV were used. This ensures that the functions involved are affected by resolution in the same way and, furthermore, the wave vectors are the same for corresponding points in energy so that the correction can be made channel by channel using the original functions. Having obtained $S_{INC}(Q,E)$ this function can now be used to obtain $S_{COH}(Q,E)$ from Eq (9') and the observed function $S^{36}(Q,E)$. Again the computation is properly done channel by channel in the case of the 20 meV data from the A-36 sample. In the case of the 15 meV data the incoherent scattering function must be interpolated in Q. The resolution broadening is slightly different for the two functions involved in this case but as the incoherent contribution to the A-36 data is small this should not give rise to significant errors.

In writing down Eqs (9) it has been assumed that the scattering functions are the same for the argon isotopes involved. Although this is not exactly true the differences are expected to be small.

VII. RESOLUTION CORRECTION

Before the data can be reduced to constant Q representation the correction for resolution broadening must be applied. The corrected spectra were obtained by the fast Fourier transform technique suggested by Cooley and Tukey [43]. The Fourier components of the data are first computed from:

$$\tilde{f}_j = \sum_{k=1}^{N} f_k \exp[i(j-1)(k-1)2\pi/N] \qquad (10)$$

where f_k are the original data points and N is a binary number chosen such that f_k is negligibly small for $k > N$. The deconvolved Fourier components are obtained by dividing the inverted data term by term by the inverted resolution function. The deconvolved spectrum, finally, is obtained by inverse transformation of the deconvolved Fourier components:

$$(f_k)_{\text{deconv.}} = \frac{1}{N} \sum_{j=1}^{N} \tilde{g}_j \cdot \exp[-i(j-1)(k-1)2\pi/N] \qquad (11)$$

where $\tilde{g}_j$ is the ratio of $\tilde{f}_j$ and the corresponding component for the resolution function. The resolution function was represented by a gaussian with the width equal to the resolution width for elastic scattering, e.g. the energy dependence of the resolution was neglected. Due to statistics the components $\tilde{f}_j$ will oscillate around 0 for large values of j while the Fourier components of the resolution function will tend smoothly to 0 when $j \to N/2$. The divided series $\tilde{g}_j$ will therefore show large fluctuations for large values of j and this will spoil the deconvolved spectrum.

To avoid this difficulty it is necessary to truncate the series $\tilde{g}_j$. The truncation, however, gives rise to ripples in the deconvolved spectrum. The amplitude of the ripples is minimized if the series is truncated at the component for which $|\tilde{g}_j|$ is minimum [44]. An example of the results obtained is shown in Fig 6a for one of the smallest angles in the case of the mixture sample. The points show the original data and the full line shows the result obtained for the deconvolved spectrum. The example shown in Fig 6a is worse than average as the spectrum in this case is very narrow. To avoid the effects of the Fourier ripples on the final data the results obtained from the decon-

volution program where smoothed by hand. In order to simplify the smoothing in the most difficult cases, e.g. the smallest angles in the case of the incoherent data, the deconvolved spectrum was first divided by a Lorentzian with FWHM equal to $2\hbar DQ^2$ where Q is the wave vector for elastic scattering and D is the diffusion constant. In this way an oscillating function with an almost constant mean value is obtained. This function was then smoothed by hand and the resulting curve was multiplied by the Lorentzian function to obtain the smoothed spectrum. The smoothing procedure is demonstrated in Fig 6b and the smoothed deconvolved spectrum is shown by the dashed line in Fig 6a. For energies larger than ~2 meV resolution correction had rather little influence on the data and therefore for $E \geq 2.2$ meV, the uncorrected data are used in the subsequent analysis.

VIII. SMOOTH SCATTERING FUNCTIONS AT CONSTANT Q

In order to obtain the scattering functions at constant values of Q the constant angle data must be interpolated. This was done by plotting the scattering function at constant energy transfer as a function of Q, drawing a smooth curve through the points and then reading off the value of the scattering function from the curve at the desired value of Q. If the data are represented in the symmetric form as given in Eq (2), both the positive and negative transfer can be used in the same constant energy plot. In the case of the coherent scattering function the data obtained at both incident energies can be used together so that the density of points is even further increased. Representative constant energy plots are shown in Fig 7 for the incoherent scattering function and in Fig 8 for the coherent scattering function. The solid lines show the smooth curves from which the scattering functions at constant Q were obtained. The consistency of the data for energy gain and energy loss is very satisfactory in the case of $S_{INC}(Q, E)$ and can be taken as a justification for the data correction procedures described above. In the case of the coherent scattering function there is a tendency for the energy gain data to be slightly lower than the energy loss data for large energy transfers. This might indicate that the multiple scattering correction, and especially the choice of kernel, is not correct for the large energy transfers in this case. From the curves shown in Figs 7 and 8 the scattering functions were obtained for Q = 1.0 - 4.4 $Å^{-1}$ in steps of 0.2 $Å^{-1}$ and, for each Q, for

E = 0.0 - 10.6 meV. In the case of the largest energies the data points do not actually extend down to Q = 1.0 $Å^{-1}$. In this case the curves were smoothly extrapolated in Q.

The final smooth scattering functions are shown in Fig 9 as functions of energy and wave vector transfer. The wellknown de-Gennes narrowing for $S_{COH}(Q, E)$ at the peaks in the structure factor is clearly displayed as is the smooth behaviour of the incoherent scattering function. The scattering functions are listed in Table III and IV. In the region E = 0.0 - 1.8 meV, the results obtained if the resolution is not corrected for are also given. In order to avoid the systematic uncertainties involved in the unfolding procedure described above, it may be desirable to fold theoretical models over the resolution function and compare the result with the uncorrected data. Although the resolution correction should actually be made on the constant angle data, the variation of the angle over the energy range where the data in the constant Q curves are significantly affected by resolution effects is small enough that the difference should be negligibly small.

As a check of the reliability of the experimental results, the energy moments for the measured scattering functions are compared to the exact theoretical results as given in Eq (4). In the case of the zeroth moment of the coherent function, for which the exact theoretical result is not known, the data by Yarnell et al. [42] were used. Fig 10a and d show the ratio of experimental to theoretical moments before the multiple and resolution corrections are applied. The effects of multiple scattering are more severe for the coherent data where, in the case of small Q, even the zeroth moment is strongly influenced. The absolute intensity of multiply scattered neutrons varies only slightly with angle but, due to the low value of S(Q) at small Q, the relative correction is very large in this case. For both scattering functions the first and second moments increase with Q and the relative importance of the multiple scattering, which is rather Q-independent, therefore decreases. The moment ratios after correction for multiple scattering and resolution are shown in Fig 10b and e. The effect of the resolution correction on the moments is small and is therefore not demonstrated separately. The experimental moments were obtained by numerical integration of the scattering functions over the energy range $-10.2 \leq E \leq 10.2$ (meV). The contribution to the moments for energy transfers larger than 10.2 meV was estimated by assuming

that $S_{INC}(Q, E)$ can be represented by the gas model in this energy range. The coherent function was represented by [6]:

$$S_{COH}(Q, E > 10.2) = S(Q) \cdot S_{GAS}(Q', E) \qquad (12)$$

with $Q' = Q/\sqrt{S(Q)}$.

With this contribution added the moment ratios are as shown in Fig 10c and f.

After correction for multiple scattering the coherent zeroth moment is everywhere within 10 per cent of the value obtained by Yarnell et al.[42] while the first and second moments are everywhere within 20 per cent of the theoretical values. In the incoherent case the zeroth moment is within 3 per cent of the theoretical value. The first moment is in this case within 10 per cent of the exact value for $Q \geq 1.4$ Å^{-1} while the maximum error in the second moment is less than 20 per cent over the same Q-range. The reason for the large deviations of the first and second moments at small Q could, at least partly, be due to a failure to account property for the resolution effects which, in this case, are large enough to influence the moments. The errors could also originate from the extrapolation of the data at small Q for large energies. In the case of the incoherent data, where only the results for $E_o = 20$ meV are used, the extrapolation is more difficult than in the case of the coherent data. We suggest that the latter effect accounts for the major part of the discrepancies.

As an overall estimate of the fulfillment of the moment relations the standard deviation σ is computed from:

$$\sigma^2 = \frac{1}{N} \sum_{i=1}^{N} \left[\frac{\langle E^n \rangle_{EXP}}{\langle E^n \rangle_{THEOR}} - 1 \right]^2 \qquad (13)$$

where the sum is over the 18 values of Q for which the experimental moments are evaluated. The results for σ are shown in Table V.

Table V

Standard deviation of moments

Incoherent			Coherent		
Zeroth	First	Second	Zeroth	First	Second
0.02	0.12	0.19	0.05	0.10	0.11

We also would like to point out again that these moment ratios are a very sensitive test of the various corrections that have been applied to the data, especially the multiple scattering correction, and the final agreement as shown in Table V is therefore most encouraging.

IX. INCOHERENT SCATTERING FUNCTION

In this Section we will discuss some features of the incoherent scattering function and compare the present results to those obtained by Levesque and Verlet [27] from molecular dynamics computations.

The main features of the incoherent function are apparent from Fig 9, in which $S_{INC}(Q, E)$ is shown to be a smooth, monotonically decreasing function of E at all values of Q. From a brief inspection of the scattering function, it is clear that the vibrational modes are heavily damped, and in fact merge with the small energy transfer region in which the diffusive modes dominate the scattering. In fact, it appears that a separation of the spectrum into a diffusive part and a vibratory part is unlikely to be fruitful as an approach to the understanding of the dynamics of liquid argon.

In Fig 11 the scattering at zero energy transfer ($S_{INC}(Q, 0)$ and the width (FWHM) of the incoherent function are compared to the simple diffusion results. For the diffusion constant the value D = $= 1.94 \cdot 10^{-5}$ cm^2/sec, which is obtained by interpolation from the values obtained by Naghizadeh and Rice [45] at 84 K and 90 K respectively, was used in all cases. Also shown in Fig 11 are the results obtained if the resolution is not corrected for. It is seen that the relative correction is very large at small values of Q, and the uncertainties in the unfolded data are therefore expected to be large at small values of Q and E.

Fig 12 shows the peak height and the width divided by the corresponding simple diffusion results. As can be seen from this figure the present results for $S_{INC}(Q, 0)$ are within 10 per cent of the simple diffusion results while the difference in the width at half maximum is less than 20 per cent at all values of Q. Also shown in Fig 12 are the molecular dynamics results by Levesque and Verlet [27]. The present neutron results and the molecular dynamics results shown the same qualitative behaviour - the width is in both cases below the simple diffusion result for Q in the range 1 - 3 Å^{-1} and is above the simple

diffusion result for larger values of Q. In fact, within the estimated uncertainties of the present results the molecular dynamics data and the neutron data are entirely consistent.

From the analysis of $S_{INC}(Q, 0)$ and of FWHM of $S_{INC}(Q, E)$ we thus conclude that the small energy transfer region agrees rather well with the simple diffusion results. In order to bring out the behaviour of the scattering function for larger energies, in Fig 13a we show the ratio of the experimental scattering function and a Lorentzian with the same width at half maximum. The general behaviour of the curves shown in Fig 13a may be summarized as follows. For $E \lesssim 2$ meV the shape of $S_{INC}(Q, E)$ is close to Lorentzian. For $2 \lesssim E \lesssim 7$ meV the scattering function shows intensity in excess of the intensity predicted by the Lorentzian shape. This is the region where the vibrational modes would be expected to show up and the "excess" intensity may be interpreted as a remnant of the phonon spectrum in the solid state. (The energy corresponding to the Debye cut-off in solid argon is ~ 7 meV.) For $E \gtrsim 7$ meV the scattering function decreases faster than the Lorentzian. However, as noted earlier, the two frequency regimes overlap completely, so that interactions between the two types of modes are clearly essential to the understanding of the overall dynamics.

As shown in Section II the intermediate scattering function $F_S(Q,t)$ is accurately described by the width function $\rho(t)$ and the first "non-Gaussian" coefficient $\alpha_2(t)$. These two quantities were derived from the present experimental scattering function in the following way. The Fourier integral in Eq (5) was evaluated numerically for a given t for all the 18 values of Q for which the scattering function is determined. The "best" values of $\rho(t)$ and $\alpha_2(t)$ were then obtained by least squares fitting of the theoretical $F_S(Q,t)$ (Eq (6)) to the "experimental" $F_S(Q,t)$ at the 18 data-points. The results obtained for $\rho(t)$ and $\alpha_2(t)$ are shown in Fig 14 together with the functions that describe the limiting behaviour of $\rho(t)$ at small and large times respectively. The crosses in Fig 14 show the experimental values for $\alpha_2(t)$. The main contribution of $\alpha_2(t)$ comes at times in the region around 10^{-12} sec. For times much larger and much smaller than 10^{-12} sec the fit is rather insensitive to the value of $\alpha_2(t)$ and the error is therefore large.

From the analysis of molecular dynamics data Levesque and Verlet [27] found that the result for $\alpha_2(t)$ is rather insensitive to the density and that a good overall fit to the high-density data could be obtained

with the function:

$$\alpha_2(t) = \frac{Ct_c}{t} \cdot e^{-(\frac{t_c}{t} - 1)} \qquad (14)$$

where C and t_c, which are both temperature dependent, are equal to 0.1186 and $1.835 \cdot 10^{-12}$ sec respectively at 85.2 K. The solid line drawn through the present result for $\alpha_2(t)$ in Fig 14 shows the result predicted by Eq (14). The circle in the $\alpha_2(t)$-plot shows the value obtained for $\alpha_2(t)$ at $t = 2.5 \cdot 10^{-12}$ sec by Rahman [7] from molecular dynamics data for T = 94.4 K. The neutron and the molecular dynamics data are again in good agreement as far as the quantitative features are concerned but the value of t_c, which is the time for which $\alpha_2(t)$ obtains the maximum value according to Eq (14), appears to be slightly higher for the molecular dynamics results.

The present results for $\rho(t)$ at small t are slightly lower than the values predicted by the free gas model. The uncertainties in the experimental results in this region of t are rather large due to termination errors in the Fourier transform and we are therefore unable to assess the significance of this difference.

The most striking feature of $\rho(t)$ is the very smooth transition from the small t behaviour to the simple diffusion behaviour which is attained already after $\sim 2 \cdot 10^{-12}$ sec. The behaviour of $\rho(t)$ suggests that the motion of the atoms in liquid argon are dominated by the diffusive motion and that, consequently, the vibrational modes are heavily damped.

X. COHERENT SCATTERING FUNCTION

The general behaviour of the coherent scattering function is obvious in the constant angle data shown in Fig 3. The narrowing of the function at angles for which the wave vector is close to a peak in the structure factor, as well as the smooth energy dependence at each angle are easily appreciated. Within the statistics and the resolution of the present experiment the curves do not show any structure but the scattering function is at all values of Q represented by a smooth peak centered at E = 0. This feature seems different from the results obtained for the coherent scattering function for liquid metals. As reported by Cocking [30] the spectra for liquid lead are dominated by

a broad peak in the inelastic region while the quasieleastic scattering has an appreciable intensity only for values of Q close to the first peak in the structure factor. Qualitatively similar results are obtained by Dahlborg and Larsson [29] for liquid aluminium although the experimental results are in this case less extensive. Both of these experiments were, however, made with neutrons of low incident energy and the results are in both cases presented as double-differential scattering cross-sections at constant angle of scattering rather than as scattering functions at constant value of the wave vector transfer. In this form the data contain the kinematic factor $((E+E_o)/E_o)^{1/2}$ (compare Eq (1)) which, if the value of E_o is small, changes rapidly over the spectrum, as does also the value of the wave vector transfer. In fact, if the present results for $S_{COH}(Q, E)$ are used to construct $d^2\sigma/d\Omega dE$ at constant angles of scattering and for the incident energy used in the lead experiment, curves similar to the ones observed by Cocking [30] are obtained. The apparent differencies in the qualitative features of the experimental results for liquid lead and liquid argon are thus artificial and due only to the different ways in which the results are presented.

The constant E curves shown in Fig 8 demonstrate very clearly the strong concentration of small energy transfer scattering to values of Q in the neighbourhood of peaks in the structure factor. As the energy transfer increases the intensity becomes more evenly distributed over the wave vector transfer and, for energies larger than ~4 meV, a dip develops at each value of Q for which S(Q) is peaked. The same effect has been observed in the data obtained for liquid lead by Randolph and Singwi [28] and also in the data by Sköld and Larsson [32] for liquid argon. In both cases the structure is well accounted for by a model in which the existence of a reciprocal lattice is assumed [46]. More specifically, the structure originates from the polarization factor which, if a reciprocal lattice is postulated, shows a Q-dependence with dips at the peaks in the structure factor. In order to explore the implications of this agreement we compare the present results with the results by Pathak and Singwi [9] in Fig 15. The theory by Pathak and Singwi, in which the structure is accounted for only by the pair-correlation function, is in good agreement with the experimental results and does indeed show the observed structure at the Q-values corresponding to the peaks in the structure factor. It is thus not necessary

to introduce explicitly the concept of a reciprocal lattice in order to explain the structure in the constant E curves.

The overall shape of $\tilde{S}_{COH}(Q, E)$ is demonstrated in Fig 13b which shows the coherent function divided by a Lorentzian of equal width for selected values of Q. A comparison with the corresponding function for the incoherent case shows that the shape of the coherent scattering function is much more Q-dependent. The excess intensity in the "inelastic" region is very large in the coherent case for values of Q for which S(Q) is small and the narrowing of $\tilde{S}_{COH}(Q, E)$ at the peaks in the structure factor is very pronounced. The narrowing is in fact much stronger than is suggested if only the width at half maximum is considered.

The differences in shape of $\tilde{S}_{INC}(Q, E)$ and $\tilde{S}_{COH}(Q, E)$ shows that convolution type approximations, e.g. the effective mass approximation [6], are unlikely to be very successful in explaining the coherent scattering.

Fig 16 shows the present results for $\tilde{S}_{COH}(Q, 0)$ together with the result predicted by various theories [1-4, 9-10]. The error bar on the experimental point for Q = 1.0 $Å^{-1}$ shows the error expected in $S_{COH}(Q, 0)$ from the uncertainty in the incoherent cross-section for the nearly coherent "A-36" sample (see discussion in Section III). For other values of Q this error is smaller than the size of the dot. The circles in Fig 16 show the result obtained if the additional correction for incoherent scattering described below is performed.

A discussion of the physical content of the theoretical models which are shown in Fig 16 is given by Pathak and Singwi [9]. In the computation of the theoretical curves the results obtained by Yarnell et al.[42] for S(Q) and g(r) were used together with a L-J potential. In cases where $S_{INC}(Q, 0)$ is needed as input to the computation the result obtained in the present experiment was used. While all models shown in Fig 16 satisfy the zeroth and second frequency moments the results by Pathak-Singwi [9], by Kurkijärvi [3] and by Ortoleva-Nelkin [4] also satisfy the fourth moment. It is seen that, on the whole, these three models give the best agreement with the data. In the convolution approximation by Vineyard [17] the peak height is given by:

$$S_{COH}(Q, 0) = S(Q) \cdot S_{INC}(Q, 0) \qquad (15)$$

In the theory of Singwi et al. [1] and in the theory of Kerr [2] the result is:

$$S_{COH}(Q, 0) = S(Q)^2 \cdot S_{INC}(Q, 0) \qquad (16)$$

e. g. the only difference between the convolution approximation and the two latter theories is in the exponent of S(Q). From a least squares fit to the experimental result we find that the best agreement is obtained if the exponent is close to 1.6. This result is obtained if the data for Q = 1.0 - 1.4 $Å^{-1}$ are disregarded in the fitting and also if, for these values of Q, the data obtained after the additional correction for incoherent scattering (open circles in Fig 16) are used. However, even with this value for the exponent the models described above (Ref [3], [4] and [9]) are closer to the experimental result.

The full width at half maximum of $S_{COH}(Q, E)$ is shown in Fig 17 with and without the resolution correction applied. Also shown in Fig 17 is the result by Pathak and Singwi [9]. The agreement between theory and experiment is not very satisfactory in this case. The disagreement is especially pronounced at small values of Q where, on the other hand, the experimental results are subject to severe systematic uncertainties. The agreement is, however, also very poor in the region around 3 $Å^{-1}$. The error bars on the experimental points for Q = 1.0 - 1.4 $Å^{-1}$ show the errors expected from the uncertainties in the incoherent cross-section for the A-36 sample (see discussion in Section III). The FWHM is very sensitive to the incoherent contribution at these values of Q and it is possible that the errors involved in this correction are underestimated. In fact, after subtracting off the incoherent scattering from the "A-36" data at the smallest scattering angles, a sharp peak with a shape very similar to the incoherent scattering function remains on top of the broad distribution which constitues the major part of the intensity. If we assume that this narrow component is indeed remaining incoherent scattering we obtain the peak heights and the widths shown as circles in Fig 16 and Fig 17 respectively. It should be noted that, although the effect on the width and on the peak height is very large, this extra incoherent component is obtained for $\sigma_{INC}/\sigma_{COH} = 0.0035$. It is therefore essential that very pure samples are used if accurate results for $\tilde{S}_{COH}(Q, E)$ should be obtained at small values of Q and E.

The result for FWHM obtained from the Pathak-Singwi model at 76 K is also shown in Fig 17. In this case the structure factor and pair-correlation function obtained by Rahman [34] at 76 K are used. A comparison of the theoretical results at the two temperatures shows that the region around Q = 1.0 $Å^{-1}$ is very sensitive to the input data. Small errors in g(r) and S(Q) could therefore cause large effects in

the theoretical width in this region of Q. Both the experimental results and the theoretical results are thus subject to large uncertainties at small values of Q and the poor agreement should therefore not be assigned undue importance. The poor agreement between theory and experiment around Q = 3 $Å^{-1}$ is, on the other hand, definitely significant and indicates a shortcoming of the Pathak-Singwi model.

It has been proposed by Rahman [34] that it may be advantageous to study the function $E^2 \cdot S_{COH}(Q, E)$, which is the frequency spectrum of the current-current correlation function, instead of the scatttering function. In particular, Rahman suggested that the value of E for which this curve has a maximum should be studied as a function of Q. In Fig 18, we show the function $E^2 \cdot S_{COH}(Q, E)$ as function of E for representative values of Q. The estimated position of the maximum (E_{max}) of the experimental curve is indicated by a vertical line in each case. The results predicted by Pathak and Singwi [9] are shown by the solid lines in Fig 18. The agreement between theory and experiment is reasonable as far as the overall shape of the curves is concerned but the theoretical curves are consistently somewhat broader and lower than the experimental curves. The values obtained for E_{max} from the experiment and from the theory are shown versus Q in Fig 19a together with the molecular dynamics result by Rahman [34]. The theoretical results show the proper qualitative behaviour and, except for regions around 1 $Å^{-1}$ and 3 $Å^{-1}$, are also in good quantitative agreement with the experimental results. The molecular dynamics results, which are for 76 K, are consistently lower than the experimental points. As can be seen from a comparison of the theoretical results for 85.2 K and for 76 K, which are also shown in Fig 19a, this discrepancy is largely explained by the difference in temperature. If the theoretical results are used to "correct" the molecular dynamics results for the difference in temperature, the molecular dynamics results and the present neutron scattering results are found to be in excellent agreement.

If the height of the $E^2 \cdot \tilde{S}_{COH}(Q, E)$ curves are used as a measure of the inverse of the energy spread the maximum value of $E^2 \cdot \tilde{S}_{COH}(Q, E)$ is a measure of the life-time of the current-current correlation [34]. This quantity is shown in Fig 19b together with the result by Rahman [34] and by Pathak and Singwi [9]. The neutron scattering results and the computer results are again in excellent agreement if the

difference in temperature is accounted for in the same way as above. The theory is in this case in reasonable qualitative agreement with the neutron results but, as observed above, is consistently lower.

XI. SUMMARY

The results reported in the present paper are the first example of experimentally obtained incoherent and coherent scattering functions for a simple monatomic liquid. It is important that both scattering functions are obtained, as the two functions illuminate different aspects of the liquid dynamics. Also, as both functions are obtained from the experiment it is now possible to test unambigously several current models for the coherent function in which the incoherent function is used as input. Although not carried out in the present paper we believe the present results to be accurate enough for a detailed quantitative comparison with theory.

In the present paper the emphasis is on the presentation of the experimental results and the various corrections that must be applied to the data before final smooth scattering functions are obtained. It is concluded that multiple scattering contamination and resolution broadening give rise to substantial distortion of the results even if great care is taken in the experiment to limit these effects. To improve the present results we suggest that an experiment should be designed such that each one of these difficulties is minimized at a time. This should be done by combining two or more series of experiments. In the small energy transfer region the resolution effects are important but the intensity is in general high. In this case it would be possible to obtain reliable data if an experiment was designed in which the resolution is substantially improved. In the large energy transfer region, where the intensity is low and the multiple scattering contamination is severe, the resolution consideration is less important. In this region, data should be obtained from an experiment in which the resolution requirements are relaxed and, instead, very thin samples are used. The complete scattering function should then be obtained from a combination of the results from these experiments, in which corrections would still be necessary but would be more reliable in each case.

The present results are in good agreement with the molecular dynamics results for both scattering functions. The mean square dis-

placement of an atom as a function of time is derived from the incoherent data. The result shows a very smooth transition from the free particle behaviour at small times to the simple diffusion behaviour which is already assumed after $\sim 2 \cdot 10^{-12}$ sec. The present result for the non-Gaussian contribution to the incoherent scattering function is in good agreement with the result obtained from molecular dynamics data by Levesque and Verlet [27] and by Rahman [7].

A recent theory for the coherent function of Pathak and Singwi [9] is in good qualitative, and in some cases quantitative, agreement with the experimental results. It is observed that the structure in the constant energy curves for momentum transfers corresponding to peaks in the structure factor is well accounted for by this model in which the concept of reciprocal lattice is not explicitly introduced. The present results for the coherent scattering function will be compared to several recent theoretical models in a forthcoming paper.

ACKNOWLEDGEMENT

The present experiment was performed at the MTR reactor at Idaho Falls. The hospitality and assistance of Dr R M Brugger, Dr W R Myers and others in the neutron scattering group at Idaho Falls is gratefully acknowledged. The preparatory work for the experiment was done at Argonne National Laboratory. For skillful technical assistance and for the design of the cryogenic equipment and the gas handling system we are most indebted to Mr R Kleb and to Mr R Stefiuk. The final analysis of the data was done at AB Atomenergi in Studsvik. We would like to thank Mr S Sandell for his assistance in the preparation of the figures. We would also like to thank Dr J L Yarnell and co-workers for allowing us to use their neutron diffraction results prior to publication.

One of us (K S) is much indebted to Dr O C Simpson and the staff at the Solid State Science Division for their hospitality during his stay at Argonne. Another (J M R) wishes to thank Dr R Pauli and the staff at AB Atomenergi, Sweden, for their hospitality during his stay at Studsvik, at which time the multiple scattering corrections were computed.

REFERENCES

1. SINGWI, K S, SKÖLD, K and TOSI, M P,
Collective motions in classical liquids.
Phys. Rev. A1 (1970) p. 454.

2. KERR, W C,
Correlated motions in simple classical liquids.
Phys. Rev. 174 (1968) p. 316.

3. KURKIJÄRVI, J,
A molecular dynamics investigation of the coherent scattering function of simple fluids.
Ann. Acad. Sci. Fenn. Ser. AVI (1970):346.

4. ORTOLEVA, P and NELKIN, M,
Fluctuations of the single-particle distribution function in classical fluids.
Phys. Rev. 181 (1969) p. 429.

5. SINGWI, K S, SKÖLD, K and TOSI, M P,
Zero sound in classical liquids.
Phys. Rev. Lett. 21 (1968) p. 881.

6. SKÖLD, K,
Small energy transfer scattering of cold neutrons from liquid argon.
Phys. Rev. Lett. 19 (1967) p. 1023.

7. RAHMAN, A,
Correlations in the motion of atoms in liquid argon.
Phys. Rev. 136A (1964) p. 405.

8. HUBBARD, J and BEEBY, J L,
Collective motion in liquids.
J. Phys. C. 2 (1969) p. 556.

9. PATHAK, K N and SINGWI, K S,
Collective motions in classical liquids II.
Phys. Rev. 2A (1970) p. 2427.

10. NELKIN, M and RANGANATHAN, S,
Collisionless sound in classical fluids.
Phys. Rev. 164 (1967) p. 222.

11. CHUNG, C H and YIP, S,
Generalized hydrodynamics and time correlation functions.
Phys. Rev. 182 (1969) p. 323.

12. AILAWADI, N K, RAHMAN, A and ZWANZIG, R,
Generalized hydrodynamics and analysis of current correlation functions.
Phys. Rev. 4A (1971) p. 1616.

13. DESAI, R C and YIP, S,
Dynamical correlations in simple liquids and cold-neutron scattering by argon.
Phys. Rev. 166 (1968) p. 129.

14. SEARS, V F,
Continued fraction representation for slow neutron scattering II.
Can. J. Phys. 48 (1970) p. 616.

15. GLASS, L and RICE, S A,
New approximation for the calculation of neutron scattering from a simple liquid.
Phys. Rev. 165 (1968) p. 186.

16. DESAI, R C and YIP, S,
Sum rule criterion in coherent slow neutron scattering in liquids.
Phys. Lett. 25A (1967).

17. DUDERSTADT, J J and AKCASU, A Z,
The calculation of current correlations in classcial fluids via modeled kinetic equations.
Phys. Rev. 2A (1970) p. 1097.

18. DESAI, R C,
Single-particle motion in simple classical liquids.
Phys. Rev. 3A (1971) p. 320.

19. AKCASU, A Z, CORNGOLD, N and DUDERSTADT, J J,
Theory of self-diffusion in classical fluids: The Van Hove self-correlation function $G_s(r,t)$.
Phys. Fluids 13 (1970) p. 2213.

20. BERNE, B J, BOON, J P and RICE, S A,
On the calculation of autocorrelation functions of dynamical variables.
J. Chem. Phys. 45 (1966) p. 1086.

21. SINGWI, K S and TOSI, M P,
On the velocity autocorrelation in a classical fluid.
Phys. Rev. 157 (1967) p. 153.

22. RAHMAN, A,
Liquid structure and self-diffusion.
J. Chem. Phys. 45 (1966) p. 2585.

23. BOON, J P and RICE, S A,
Memory effects and the autocorrelation function of a dynamical variable.
J. Chem. Phys. 47 (1967) p. 2480.

24. SINGWI, K S and SJÖLANDER, A,
Theory of atomic motions in simple classical liquids.
Phys. Rev. 167 (1968) p. 152.

25. MARTIN, P C and YIP, S,
Frequency-dependent friction constant analysis of diffusion in simple liquids.
Phys. Rev. 170 (1968) p. 151.

26. CORNGOLD, N and DUDERSTADT, J J,
Perturbative theory of self-diffusion in classical many-particle systems. I. Velocity autocorrelation function.
Phys. Rev. 2A (1970) p. 836.

27. LEVESQUE, D and VERLET, L,
Computer "experiments" on classical fluids. III. Time-dependent self-correlation functions.
Phys. Rev. 2A (1970) p. 2514.

28. RANDOLPH, P D and SINGWI, K S,
Slow-neutron scattering and collective motions in liquid lead.
Phys. Rev. 152 (1966) p. 99.

29. DAHLBORG, U and LARSSON, K E,
Collective atomic motions in liquid aluminium studied by cold neutron scattering.
Arkiv Fysik 33 (1967) p. 271.

30. COCKING, S J,
Studies of the liquid state using the inelastic scattering of slow neutrons. 1968.
(AERE-R5867) Thesis. Submitted to University of London.

31. LARSSON, K E,
Liquid dynamics from neutron scattering.
Neutron inelastic scattering. Proc. of a symp. Copenhagen, 20 - 25 May, 1968. (IAEA), Vienna 1968, Vol. I, p. 397.

32. SKÖLD, K and LARSSON, K E,
Atomic motion in liquid argon.
Phys. Rev. 161 (1967) p. 102.

33. CHEN, S H et al.,
Co-operative modes of motion in simple liquids.
Phys. Lett. 19 (1965) p. 269.

34. RAHMAN, A,
Current fluctuations in classical liquids.
Neutron inelastic scattering. Proc. of a symp. Copenhagen, 20 - 25 May, 1968. (IAEA), Vienna 1968, Vol. 1, p. 561.

35. NIJBOER, B R A and RAHMAN, A,
Time expansion of correlation functions and the theory of slow neutron scattering.
Physica 32 (1966) p. 415.

36. VINEYARD, G H,
Multiple scattering of neutrons.
Phys. Rev. 96 (1954) p. 93.

37. COCKING, S J and HEARD, C R T,
Multiple scattering in plane samples: Application to scattering of thermal neutrons. 1965.
(AERE-R5016).

38. SLAGGIE, E L,
a) Multiple scattering in slow-neutron double-differential measurements.
Nucl. Sci. Eng. 30 (1967) p. 199.

b) Multiple scattering in neutron double-differential cross-section measurements.
Neutron thermalization and reactor spectra. Proc. of a symp. Ann Arbor 17 - 21 July, 1967. (IAEA), Vienna 1968. Vol. 1, p. 311.

c) Multiple scattering in double-differential measurements as a function of neutron path length.
Nucl. Sci. Eng. 36 (1969) p. 105.

39. BLECH, I A and AVERBACH, B L,
Multiple scattering of neutrons in vanadium and copper.
Phys. Rev. 137A (1965) p. 1113.

40. BISCHOFF, F G, YEATER, M L and MOORE, W E,
Monte Carlo evaluation of multiple scattering and resolution effects in double-differential neutron scattering cross section measurements. 1970.
(RPI-328-211) Thesis. Submitted to Rensselaer Polytechnic Inst., Troy, N. Y., by F G Bischoff.

41. BRUGGER, R M,
Slow neutron scattering from water.
Nucl. Sci. Eng. 33 (1968) p. 187.

42. YARNELL, J L et al.,
(To be published.)

43. COOLEY, J W and TUKEY, J W,
An algorithm for the machine calculation of complex Fourier series.
Math. Comput. 19 (1965) p. 297.

44. BREGMAN, J D and de MUL, F F M,
Intermediate scattering functions obtained by fast Fourier transformation of cold neutron time-of-flight spectra.
Nucl. Instr. Methods 93 (1971) p. 109.

45. NAGHIZADEH, J and RICE, S A,
Kinetic theory of dense fluids. X. Measurement and interpretation of self-diffusion in liquid Ar, Kr, Xe, and CH_4.
J. Chem. Phys. 36 (1962) p. 2710.

46. EGELSTAFF, P A,
The scattering of cold neutrons by metals. 1962.
(AERE- R4101.)

47. VINEYARD, G H,
Scattering of slow neutrons by a liquid.
Phys. Rev. 110 (1958) p. 999.

48. KROHN, V E and RINGO, G R,
Measurement of the electron-neutron interaction by the asymmetrical scattering of thermal neutrons by noble gases.
Phys. Rev. 148 (1966) p. 1303.

Table III

Incoherent scattering function: $\tilde{S}_{INC}(Q, E)$

Data are corrected for multiple scattering and, except for the data in brackets, for resolution broadening.

Q(Å^{-1}) / ΔE (meV)	1.0	1.2	1.4	1.6	1.8	2.0	2.2	2.4	2.6
0.0	2.7500 (0.9750)	1.8000 (0.8350)	1.2500 (0.7300)	0.9500 (0.6550)	0.7700 (0.5900)	0.6450 (0.5000)	0.5400 (0.4250)	0.4500 (0.3700)	0.3700 (0.3250)
0.2	0.6100 (0.7150)	0.6950 (0.6950)	0.7500 (0.6700)	0.7000 (0.6100)	0.6100 (0.5350)	0.5250 (0.4700)	0.4500 (0.4000)	0.4000 (0.3400)	0.3400 (0.2950)
0.4	0.1250 (0.5060)	0.2380 (0.4890)	0.3150 (0.4700)	0.3670 (0.4460)	0.3920 (0.4180)	0.3680 (0.3790)	0.3340 (0.3430)	0.3030 (0.3100)	0.2750 (0.2780)
0.6	0.0750 (0.3520)	0.1350 (0.2690)	0.1820 (0.2820)	0.2210 (0.2880)	0.2510 (0.2880)	0.2600 (0.2850)	0.2500 (0.2690)	0.2380 (0.2510)	0.2250 (0.2320)
0.8	0.0655 (0.1180)	0.0950 (0.1450)	0.1230 (0.1690)	0.1470 (0.1870)	0.1660 (0.2030)	0.1790 (0.2080)	0.1825 (0.2060)	0.1820 (0.2010)	0.1800 (0.1940)
1.0	0.0555 (0.0670)	0.0690 (0.0860)	0.0830 (0.1050)	0.0980 (0.1210)	0.1140 (0.1360)	0.1290 (0.1490)	0.1440 (0.1560)	0.1540 (0.1600)	0.1545 (0.1590)
1.2	0.0415 (0.0420)	0.0500 (0.0560)	0.0600 (0.0730)	0.0735 (0.0920)	0.0875 (0.1080)	0.1010 (0.1100)	0.1135 (0.1300)	0.1240 (0.1370)	0.1275 (0.1330)
1.4	0.0285 (0.0320)	0.0395 (0.0440)	0.0495 (0.0560)	0.0595 (0.0680)	0.0710 (0.0780)	0.0850 (0.0918)	0.0965 (0.1055)	0.1015 (0.1135)	0.1040 (0.1130)
1.6	0.0215 (0.0260)	0.0335 (0.0360)	0.0435 (0.0460)	0.0510 (0.0545)	0.0600 (0.0620)	0.0710 (0.0720)	0.0815 (0.0825)	0.0850 (0.0875)	0.0875 (0.0920)
1.8	0.0180 (0.0235)	0.0255 (0.0300)	0.0345 (0.0370)	0.0495 (0.0440)	0.0585 (0.0515)	0.0645 (0.0640)	0.0740 (0.0770)	0.0760 (0.0800)	0.0750 (0.0780)
2.2	0.0160	0.0195	0.0240	0.0305	0.0375	0.0465	0.0550	0.0615	0.0670
2.6	0.0110	0.0145	0.0190	0.0235	0.0290	0.0340	0.0400	0.0460	0.0500
3.0	0.0090	0.0114	0.0139	0.0170	0.0206	0.0244	0.0314	0.0394	0.0418
3.4	0.0072	0.0090	0.0107	0.0129	0.0154	0.0185	0.0248	0.0307	0.0332
3.8	0.0054	0.0070	0.0085	0.0103	0.0125	0.0157	0.0200	0.0237	0.0269
4.2	0.0041	0.0053	0.0067	0.0083	0.0102	0.0126	0.0165	0.0196	0.0222
4.6	0.0032	0.0041	0.0051	0.0063	0.0084	0.0109	0.0137	0.0165	0.0189
5.0	0.0026	0.0033	0.0041	0.0054	0.0072	0.0088	0.0114	0.0136	0.0157
5.4	0.0023	0.0028	0.0033	0.0042	0.0054	0.0074	0.0097	0.0116	0.0134
5.8	0.0021	0.0023	0.0026	0.0034	0.0047	0.0061	0.0080	0.0102	0.0115
6.2	0.0020	0.0020	0.0020	0.0027	0.0032	0.0046	0.0061	0.0077	0.0090
6.6	0.0015	0.0016	0.0018	0.0021	0.0026	0.0038	0.0053	0.0067	0.0081
7.0	0.0013	0.0015	0.0016	0.0018	0.0019	0.0026	0.0036	0.0049	0.0063
7.4	0.0010	0.0010	0.0010	0.0011	0.0012	0.0018	0.0027	0.0038	0.0051
7.8	0.0008	0.0008	0.0008	0.0008	0.0008	0.0012	0.0018	0.0029	0.0041
8.2	0.0005	0.0005	0.0005	0.0005	0.0007	0.0011	0.0017	0.0024	0.0033
8.6	0.0004	0.0004//	0.0004	0.0005	0.0006	0.0008	0.0011	0.0018	0.0025
9.0	0.0003	0.0003	0.0003	0.0003	0.0003	0.0004	0.0008	0.0014	0.0019
9.4	0.0001	0.0001	0.0001	0.0002	0.0002	0.0003	0.0005	0.0008	0.0012
9.8	0.0000	0.0000	0.0000	0.0000	0.0000	0.0001	0.0004	0.0007	0.0012
10.2	0.0000	0.0000	0.0000	0.0000	0.0000	0.0000	0.0001	0.0004	0.0008
10.6	0.0000	0.0000	0.0000	0.0000	0.0000	0.0000	0.0000	0.0001	0.0003

Cont.

Table III cont.

Q(Å^{-1}) / ΔE (meV)	2.8	3.0	3.2	3.4	3.6	3.8	4.0	4.2	4.4
0.0	0.3030 (0.2800)	0.2600 (0.2400)	0.2330 (0.2200)	0.2120 (0.2000)	0.1920 (0.1800)	0.1750 (0.1650)	0.1580 (0.1500)	0.1440 (0.1400)	0.1340 (0.1350)
0.2	0.2900 (0.2600)	0.2520 (0.2350)	0.2270 (0.2150)	0.2070 (0.2000)	0.1890 (0.1850)	0.1730 (0.1700)	0.1590 (0.1600)	0.1450 (0.1450)	0.1330 (0.1320)
0.4	0.2500 (0.2480)	0.2300 (0.2230)	0.2140 (0.2080)	0.2010 (0.1960)	0.1870 (0.1780)	0.1740 (0.1620)	0.1600 (0.1540)	0.1450 (0.1440)	0.1290 (0.1260)
0.6	0.2130 (0.2140)	0.2010 (0.2000)	0.1900 (0.1900)	0.1800 (0.1800)	0.1690 (0.1680)	0.1590 (0.1560)	0.1480 (0.1460)	0.1370 (0.1350)	0.1250 (0.1230)
0.8	0.1760 (0.1860)	0.1710 (0.1770)	0.1660 (0.1680)	0.1600 (0.1610)	0.1530 (0.1540)	0.1450 (0.1460)	0.1370 (0.1370)	0.1300 (0.1280)	0.1220 (0.1190)
1.0	0.1510 (0.1550)	0.1480 (0.1510)	0.1440 (0.1460)	0.1400 (0.1420)	0.1360 (0.1370)	0.1300 (0.1320)	0.1250 (0.1270)	0.1200 (0.1200)	0.1140 (0.1140)
1.2	0.1280 (0.1280)	0.1285 (0.1280)	0.1285 (0.1290)	0.1275 (0.1280)	0.1245 (0.1250)	0.1200 (0.1210)	0.1160 (0.1170)	0.1120 (0.1130)	0.1070 (0.1090)
1.4	0.1070 (0.1125)	0.1095 (0.1155)	0.1115 (0.1175)	0.1130 (0.1180)	0.1125 (0.1160)	0.1110 (0.1125)	0.1085 (0.1085)	0.1055 (0.1045)	0.1020 (0.1010)
1.6	0.0925 (0.0960)	0.0980 (0.1005)	0.1020 (0.1045)	0.1035 (0.1065)	0.1035 (0.1050)	0.1025 (0.1020)	0.1010 (0.0995)	0.0990 (0.0970)	0.0970 (0.0950)
1.8	0.0810 (0.0810)	0.0890 (0.0875)	0.0935 (0.0935)	0.0960 (0.0970)	0.0950 (0.0955)	0.0950 (0.0940)	0.0945 (0.0925)	0.0930 (0.0915)	0.0910 (0.0905)
2.2	0.0710	0.0740	0.0775	0.0800	0.0835	0.0870	0.0865	0.0825	0.0785
2.6	0.0540	0.0580	0.0625	0.0665	0.0695	0.0720	0.0725	0.0725	0.0720
3.0	0.0439	0.0479	0.0521	0.0562	0.0592	0.0613	0.0626	0.0637	0.0643
3.4	0.0355	0.0390	0.0440	0.0477	0.0502	0.0521	0.0538	0.0553	0.0566
3.8	0.0301	0.0336	0.0370	0.0462	0.0426	0.0448	0.0470	0.0490	0.0505
4.2	0.0249	0.0278	0.0307	0.0335	0.0361	0.0386	0.0409	0.0430	0.0448
4.6	0.0212	0.0236	0.0262	0.0286	0.0310	0.0335	0.0358	0.0380	0.0400
5.0	0.0177	0.0203	0.0229	0.0251	0.0271	0.0292	0.0313	0.0335	0.0353
5.4	0.0154	0.0173	0.0192	0.0211	0.0230	0.0251	0.0275	0.0296	0.0310
5.8	0.0131	0.0147	0.0164	0.0183	0.0201	0.0219	0.0238	0.0254	0.0267
6.2	0.0105	0.0123	0.0140	0.0156	0.0172	0.0188	0.0203	0.0218	0.0232
6.6	0.0093	0.0105	0.0116	0.0130	0.0148	0.0161	0.0173	0.0185	0.0197
7.0	0.0077	0.0088	0.0097	0.0110	0.0125	0.0137	0.0147	0.0157	0.0172
7.4	0.0062	0.0071	0.0079	0.0090	0.0102	0.0114	0.0127	0.0141	0.0155
7.8	0.0052	0.0059	0.0065	0.0073	0.0085	0.0097	0.0109	0.0122	0.0135
8.2	0.0042	0.0048	0.0053	0.0060	0.0069	0.0081	0.0094	0.0108	0.0121
8.6	0.0039	0.0040	0.0044	0.0050	0.0060	0.0070	0.0081	0.0093	0.0105
9.0	0.0025	0.0031	0.0036	0.0044	0.0056	0.0060	0.0071	0.0081	0.0092
9.4	0.0017	0.0023	0.0030	0.0036	0.0042	0.0050	0.0059	0.0069	0.0079
9.8	0.0016	0.0021	0.0026	0.0032	0.0039	0.0046	0.0053	0.0062	0.0070
10.2	0.0012	0.0018	0.0023	0.0029	0.0035	0.0041	0.0048	0.0055	0.0062
10.6	0.0007	0.0011	0.0016	0.0020	0.0024	0.0028	0.0033	0.0037	0.0042

Table IV

Coherent scattering function: $\tilde{S}_{COH}(Q, E)$

Data are corrected for multiple scattering and, except for the data in brackets, for resolution broadening.

$Q(Å^{-1})$ / ΔE (meV)	1.0	1.2	1.4	1.6	1.8	2.0	2.2	2.4	2.6
0.0	0.0240 (0.0220)	0.0360 (0.0320)	0.0580 (0.0560)	0.1800 (0.1500)	1.1000 (0.8400)	2.4000 (1.7900)	0.6100 (0.5300)	0.2250 (0.2000)	0.1390 (0.2100)
0.2	0.0215 (0.0200)	0.0300 (0.0290)	0.0550 (0.0510)	0.1550 (0.1420)	0.8500 (0.7000)	1.9800 (1.6550)	0.5400 (0.5000)	0.2000 (0.2000)	0.1280 (0.2150)
0.4	0.0175 (0.0185)	0.0235 (0.0250)	0.0470 (0.0435)	0.1200 (0.1250)	0.4750 (0.5500)	1.1150 (1.2200)	0.4200 (0.4400)	0.1900 (0.1850)	0.1200 (0.1900)
0.6	0.0140 (0.0145)	0.0200 (0.0190)	0.0400 (0.0380)	0.1100 (0.1025)	0.3400 (0.3750)	0.5600 (0.8000)	0.3400 (0.3450)	0.1600 (0.1600)	0.0960 (0.1700)
0.8	0.0124 (0.0124)	0.0160 (0.0183)	0.0320 (0.0325)	0.0840 (0.0830)	0.2400 (0.2700)	0.3620 (0.4900)	0.2540 (0.2800)	0.1330 (0.1400)	0.0880 (0.1500)
1.0	0.0112 (0.0108)	0.0140 (0.0173)	0.0270 (0.0296)	0.0660 (0.0710)	0.1840 (0.1940)	0.2820 (0.3250)	0.1960 (0.2220)	0.1140 (0.1130)	0.0800 (0.1230)
1.2	0.0100 (0.0085)	0.0125 (0.0150)	0.0230 (0.0248)	0.0560 (0.0580)	0.1400 (0.1340)	0.2050 (0.2300)	0.1620 (0.1700)	0.0980 (0.1070)	0.0720 (0.1070)
1.4	0.0088 (0.0086)	0.0118 (0.0130)	0.0224 (0.0200)	0.0490 (0.0520)	0.1050 (0.1100)	0.1480 (0.1670)	0.1350 (0.1400)	0.0880 (0.0930)	0.0630 (0.0960)
1.6	0.0080 (0.0080)	0.0110 (0.0112)	0.0190 (0.0198)	0.0435 (0.0440)	0.0795 (0.0870)	0.1175 (0.1280)	0.1110 (0.1200)	0.0800 (0.0800)	0.0590 (0.0860)
1.8	0.0070 (0.0068)	0.0100 (0.0120)	0.0160 (0.0173)	0.0360 (0.0350)	0.0665 (0.0690)	0.1000 (0.1000)	0.0950 (0.1000)	0.0705 (0.0730)	0.0495 (0.0780)
2.2	0.0050	0.0080	0.0135	0.0285	0.0490	0.0620	0.0655	0.0555	0.0415
2.6	0.0035	0.0060	0.0120	0.0235	0.0345	0.0450	0.0495	0.0405	0.0365
3.0	0.0028	0.0060	0.0112	0.0188	0.0264	0.0318	0.0394	0.0380	0.0335
3.4	0.0027	0.0050	0.0095	0.0145	0.0180	0.0225	0.0290	0.0300	0.0285
3.8	0.0028	0.0049	0.0081	0.0114	0.0134	0.0163	0.0212	0.0230	0.0254
4.2	0.0027	0.0047	0.0070	0.0091	0.0100	0.0118	0.0187	0.0201	0.0217
4.6	0.0026	0.0042	0.0059	0.0072	0.0079	0.0090	0.0127	0.0163	0.0186
5.0	0.0024	0.0037	0.0051	0.0058	0.0059	0.0067	0.0100	0.0136	0.0165
5.4	0.0018	0.0032	0.0044	0.0050	0.0048	0.0055	0.0080	0.0114	0.0136
5.8	0.0015	0.0026	0.0035	0.0036	0.0036	0.0043	0.0062	0.0096	0.0113
6.2	0.0015	0.0022	0.0030	0.0026	0.0025	0.0033	0.0052	0.0087	0.0096
6.6	0.0017	0.0021	0.0022	0.0021	0.0019	0.0022	0.0040	0.0062	0.0079
7.0	0.0014	0.0019	0.0021	0.0017	0.0013	0.0015	0.0030	0.0048	0.0065
7.4	0.0012	0.0016	0.0016	0.0013	0.0012	0.0012	0.0021	0.0036	0.0051
7.8	0.0009	0.0013	0.0014	0.0011	0.0008	0.0009	0.0014	0.0020	0.0035
8.2	0.0009	0.0012	0.0012	0.0011	0.0009	0.0008	0.0013	0.0020	0.0030
8.6	0.0009	0.0010	0.0010	0.0010	0.0009	0.0008	0.0009	0.0013	0.0022
9.0	0.0007	0.0009	0.0009	0.0009	0.0009	0.0009	0.0009	0.0011	0.0016
9.4	0.0005	0.0007	0.0008	0.0008	0.0008	0.0007	0.0009	0.0012	0.0016
9.8	0.0003	0.0005	0.0007	0.0008	0.0008	0.0008	0.0009	0.0012	0.0015
10.2	0.0002	0.0004	0.0005	0.0006	0.0007	0.0006	0.0008	0.0015	0.0017
10.6	0.0000	0.0002	0.0004	0.0006	0.0006	0.0005	0.0011	0.0015	0.0015

Cont.

Table IV cont.

ΔE (meV) \ Q(Å^{-1})	2.8	3.0	3.2	3.4	3.6	3.8	4.0	4.2	4.4
0.0	0.1350 (0.2550)	0.1790 (0.1300)	0.2250 (0.1250)	0.2700 (0.1550)	0.2730 (0.2600)	0.2230 (0.2200)	0.1730 (0.1700)	0.1330 (0.1280)	0.1050 (0.0950)
0.2	0.1200 (0.2500)	0.1700 (0.1170)	0.2150 (0.1100)	0.2570 (0.1550)	0.2630 (0.2500)	0.2220 (0.2100)	0.1720 (0.1700)	0.1240 (0.1200)	0.0990 (0.0950)
0.4	0.1000 (0.2300)	0.1550 (0.1100)	0.2000 (0.1000)	0.2350 (0.1450)	0.2450 (0.2420)	0.2150 (0.2100)	0.1700 (0.1550)	0.1150 (0.1220)	0.0930 (0.0950)
0.6	0.0960 (0.2050)	0.1320 (0.1000)	0.1700 (0.0950)	0.2060 (0.1270)	0.2220 (0.2200)	0.1980 (0.1950)	0.1560 (0.1550)	0.1140 (0.1150)	0.0900 (0.0900)
0.8	0.0920 (0.1880)	0.1080 (0.0900)	0.1440 (0.0900)	0.1810 (0.1120)	0.2020 (0.2060)	0.1840 (0.1840)	0.1440 (0.1440)	0.1110 (0.1100)	0.0840 (0.0860)
1.0	0.0840 (0.1640)	0.0910 (0.0810)	0.1200 (0.0790)	0.1620 (0.0930)	0.1860 (0.1850)	0.1680 (0.1650)	0.1330 (0.1330)	0.1040 (0.1030)	0.0820 (0.0830)
1.2	0.0760 (0.1460)	0.0770 (0.0720)	0.1050 (0.0730)	0.1440 (0.0820)	0.1630 (0.1670)	0.1530 (0.1520)	0.1220 (0.1200)	0.0960 (0.0980)	0.0800 (0.0790)
1.4	0.0660 (0.1280)	0.0690 (0.0660)	0.0930 (0.0630)	0.1300 (0.0710)	0.1470 (0.1480)	0.1420 (0.1390)	0.1120 (0.1150)	0.0900 (0.0930)	0.0770 (0.0780)
1.6	0.0585 (0.1140)	0.0635 (0.0600)	0.0865 (0.0590)	0.1125 (0.0665)	0.1325 (0.1370)	0.1305 (0.1300)	0.1040 (0.1060)	0.0900 (0.0880)	0.0735 (0.0740)
1.8	0.0525 (0.1030)	0.0585 (0.0520)	0.0785 (0.0530)	0.1000 (0.0590)	0.1185 (0.1225)	0.1195 (0.1170)	0.0985 (0.0975)	0.0815 (0.0800)	0.0700 (0.0680)
2.2	0.0465	0.0490	0.0620	0.0805	0.0985	0.0995	0.0845	0.0745	0.0630
2.6	0.0395	0.0410	0.0510	0.0650	0.0790	0.0855	0.0740	0.0645	0.0575
3.0	0.0325	0.0350	0.0440	0.0540	0.0650	0.0700	0.0645	0.0585	0.0530
3.4	0.0280	0.0310	0.0370	0.0450	0.0540	0.0585	0.0570	0.0540	0.0485
3.8	0.0242	0.0270	0.0315	0.0371	0.0438	0.0494	0.0484	0.0452	0.0435
4.2	0.0214	0.0233	0.0269	0.0314	0.0365	0.0404	0.0416	0.0411	0.0396
4.6	0.0186	0.0199	0.0230	0.0266	0.0306	0.0338	0.0357	0.0362	0.0350
5.0	0.0160	0.0170	0.0196	0.0224	0.0253	0.0281	0.0306	0.0322	0.0316
5.4	0.0147	0.0156	0.0166	0.0180	0.0205	0.0234	0.0270	0.0286	0.0282
5.8	0.0126	0.0137	0.0145	0.0152	0.0168	0.0196	0.0226	0.0248	0.0251
6.2	0.0108	0.0117	0.0123	0.0128	0.0140	0.0167	0.0193	0.0213	0.0222
6.6	0.0092	0.0103	0.0107	0.0105	0.0113	0.0143	0.0171	0.0186	0.0193
7.0	0.0077	0.0087	0.0090	0.0088	0.0098	0.0118	0.0143	0.0159	0.0168
7.4	0.0063	0.0074	0.0078	0.0077	0.0078	0.0084	0.0109	0.0137	0.0146
7.8	0.0054	0.0063	0.0065	0.0063	0.0068	0.0084	0.0102	0.0115	0.0126
8.2	0.0041	0.0050	0.0056	0.0057	0.0060	0.0072	0.0087	0.0099	0.0112
8.6	0.0032	0.0041	0.0046	0.0048	0.0050	0.0056	0.0071	0.0084	0.0097
9.0	0.0025	0.0032	0.0038	0.0041	0.0043	0.0045	0.0056	0.0070	0.0085
9.4	0.0018	0.0022	0.0029	0.0032	0.0032	0.0033	0.0040	0.0054	0.0068
9.8	0.0017	0.0016	0.0021	0.0027	0.0028	0.0030	0.0033	0.0042	0.0058
10.2	0.0015	0.0011	0.0015	0.0023	0.0025	0.0025	0.0025	0.0034	0.0049
10.6	0.0012	0.0007	0.0013	0.0020	0.0021	0.0019	0.0020	0.0030	0.0042

FIGURE CAPTIONS

Fig 1a The solid and the dashed curves show the trace in the E-Q plane for the smallest and largest scattering angles for both incident energies. The dashed rectangle shows the area over which smooth scattering functions are obtained.

Fig 1b Standard deviation of energy resolution function for elastic scattering for both incident energies.

Fig 1c Standard deviation of wave vector transfer resolution function for elastic scattering for both incident energies and the structure factor S(Q).

Fig 2 Observed intensity at selected angles for the three samples measured. The normalized intensity from the empty container is shown by the solid line in each case.

Fig 3 Double differential scattering cross-sections at selected angles for the three samples measured. The solid lines show the resolution function in each case.

Fig 4 Double differential scattering cross-section at small, medium and large scattering angle are shown for the three measurements together with the multiple scattering contribution (solid lines). "Second" and "third" are the contributions from neutrons scattered two and three times respectively.

Fig 5 The present result for the structure factor before and after the multiple scattering correction is applied compared to the neutron diffraction result by Yarnell et al. [42].

Fig 6 a, b Solid dots in Fig 6a show the spectrum observed at $\theta = 34.17^{\circ}$ from the mixture sample. The solid line shows the result obtained for the resolution corrected spectrum from the Fourier transform program. The solid line in Fig 6b shows the same curve divided by a Lorentzian function with the same width. The dashed curves in Fig 6a and 6b show the result of the smoothing described in the text.

Fig 7 Final corrected incoherent scattering function versus Q for selected values of E. The smooth scattering function at

constant Q is obtained from the solid curves drawn through the data points.

Fig 8 Final corrected coherent scattering function versus Q for selected values of E. The smooth scattering function at constant Q is obtained from the solid curves drawn through the data points.

Fig 9 Smooth scattering functions shown versus Q and E. The dashed line and the solid line show the envelope of the incoherent and the coherent scattering functions respectively.

Fig 10 a, d Zeroth, first and second energy moments of experimental scattering functions divided by theoretical moments before correcting the data for multiple scattering and resolution for the incoherent and the coherent data respectively. For the theoretical zeroth moment in the coherent case the experimental result by Yarnell et al. [42] is used.

Fig 10 b, e Same as Fig 10a, d but after correcting the data for multiple scattering and resolution.

Fig 10 c, f Same as Fig 10b, e but after extrapolation of the moment integral as explained in the text.

Fig 11a Full width at half maximum of the incoherent scattering function before and after the resolution correction. Also shown is the simple diffusion result with $D = 1.94 \cdot 10^{-5}$ cm^2/sec [45].

Fig 11b Intensity at zero energy transfer for the incoherent scattering function before and after the resolution correction. The solid line shows the simple diffusion result.

Fig 12 a, b FWHM and $S_{INC}(Q, 0)$ divided by the simple diffusion results are shown together with the molecular dynamics results by Levesque and Verlet [27].

Fig 13a Incoherent scattering function divided by a Lorentzian of the same width is shown for selected values of Q.

Fig 13b Coherent scattering function divided by a Lorentzian of the same width is shown for selected values of Q.

Fig 14 $\rho(t)$ and $\alpha_2(t)$ (scale to the right) from the present experiment. The limiting behaviour of $\rho(t)$ at small and large times as obtained for a free gas and for simple diffusion respectively are also shown. The solid line in the $\alpha_2(t)$-plot shows the result obtained by Levesque and Verlet [27]. The circle shows the result obtained by Rahman [7] for $\alpha_2(t)$ at $t = 2.5 \cdot 10^{-12}$ sec for argon at 94.4 K.

Fig 15 Comparison of present result for $\tilde{S}_{COH}(Q, E)$ at constant E and the result obtained by Pathak and Singwi [9].

Fig 16 The present result for $\tilde{S}_{COH}(Q, 0)$ compared to various theoretical predictions. The error bar on the point at $Q = 1.0$ Å^{-1} shows the uncertainties in $\tilde{S}_{COH}(Q, 0)$ due to the uncertainties in σ_{INC} for the "A-36" sample. For other values of Q this error is smaller than the size of the dot. The circles at $Q = 1.0$, 1.2 and 1.4 Å^{-1} show the result if the additional correction for the incoherent contribution described in the text is applied.

Fig 17 Full width at half maximum of $\tilde{S}_{COH}(Q, E)$ before and after applying the resolution correction. The error bars on the data at $Q = 1.0$, 1.2 and 1.4 Å^{-1} show the uncertainties in FWHM due to the uncertainties in σ_{INC} for the "A-36" sample. The circles at the same values of Q show the result for FWHM if the additional correction for the incoherent contribution described in the text is applied. The theoretical results are for S(Q) and g(r) from molecular dymics [34] (76 K) and from neutron diffraction [42] (85.2 K) respectively. In both cases a L-J potential is assumed.

Fig 18 The function $E^2 \cdot \tilde{S}_{COH}(Q, E)$ from the present experiment and from the theory by Pathak and Singwi [9] with S(Q) and g(r) from neutron diffraction (Yarnell et al. [42]). The vertical lines show the estimated positions of the maxima in the experimental curves.

Fig 19a The present results for E_{max} and those obtained from the molecular dynamics computations by Rahman [34] at 76 K are

compared to the theoretical results by Pathak and Singwi [9]. The theoretical results are for S(Q) and g(r) from molecular dynamics [34] (76 K) and from neutron diffraction [42] (85.2 K) respectively. In both cases a L-J potential is assumed.

Fig 19b Maximum value of $E^2 \cdot \tilde{S}_{COH}(Q, E)$ divided by $\langle E^2 \rangle$ from the present experiment and from the molecular dynamics computations by Rahman [34] at 76 K are compared to the theoretical results by Pathak and Singwi [9]. The theoretical results are for S(Q) and g(r) from molecular dynamics [34] (76 K) and from neutron diffraction [42] (85.2 K) respectively In both cases a L-J potential is assumed.

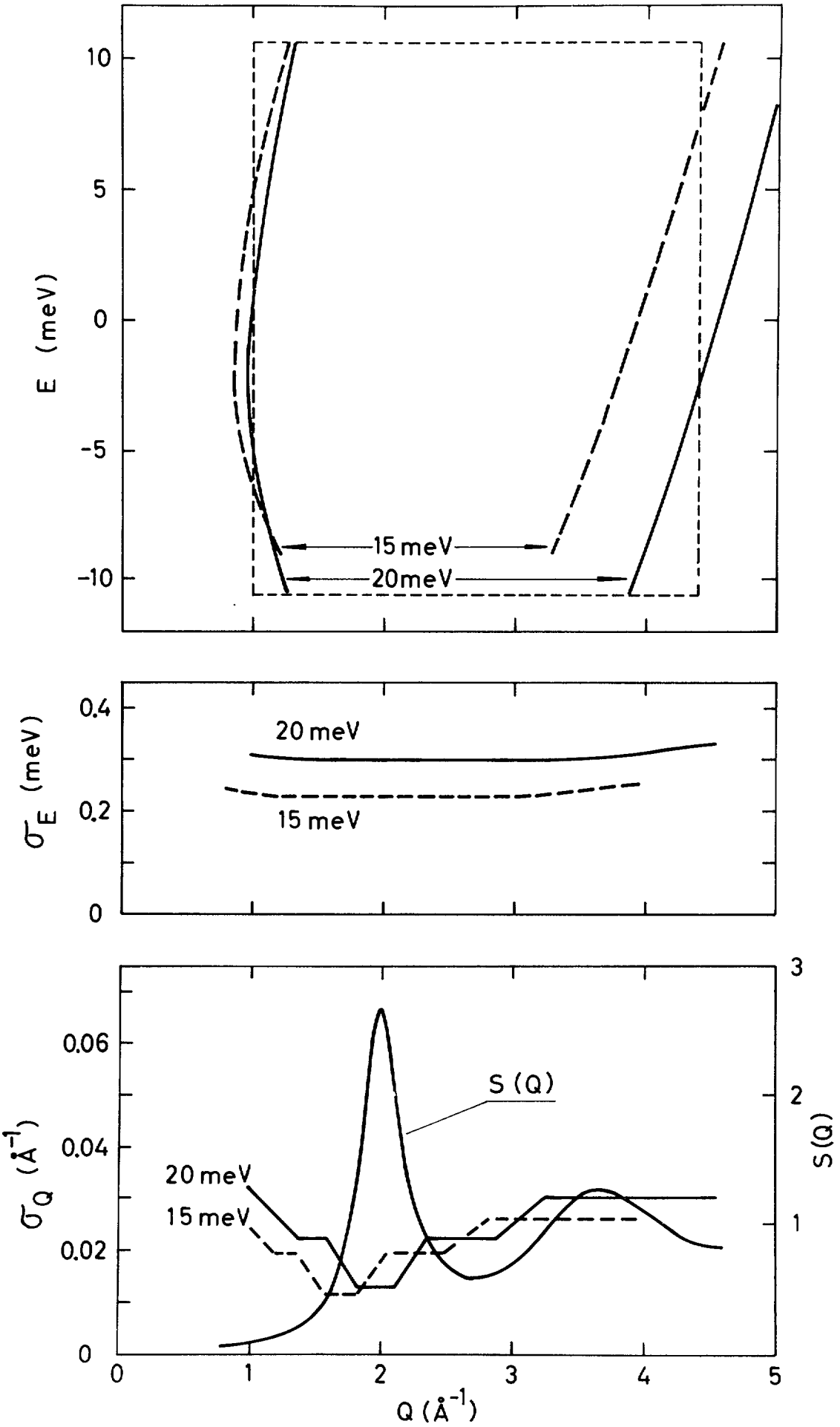
10
5
0
-5
-10
E (meV)
15 meV
20meV
0.4
0.2
0
σ_E (meV)
20 meV
15 meV
0.06
0.04
0.02
0
σ_Q (Å^{-1})
S (Q)
20 meV
15 meV
3
2
1
S(Q)
0
1
2
3
4
5
Q (Å^{-1})

Figure 1

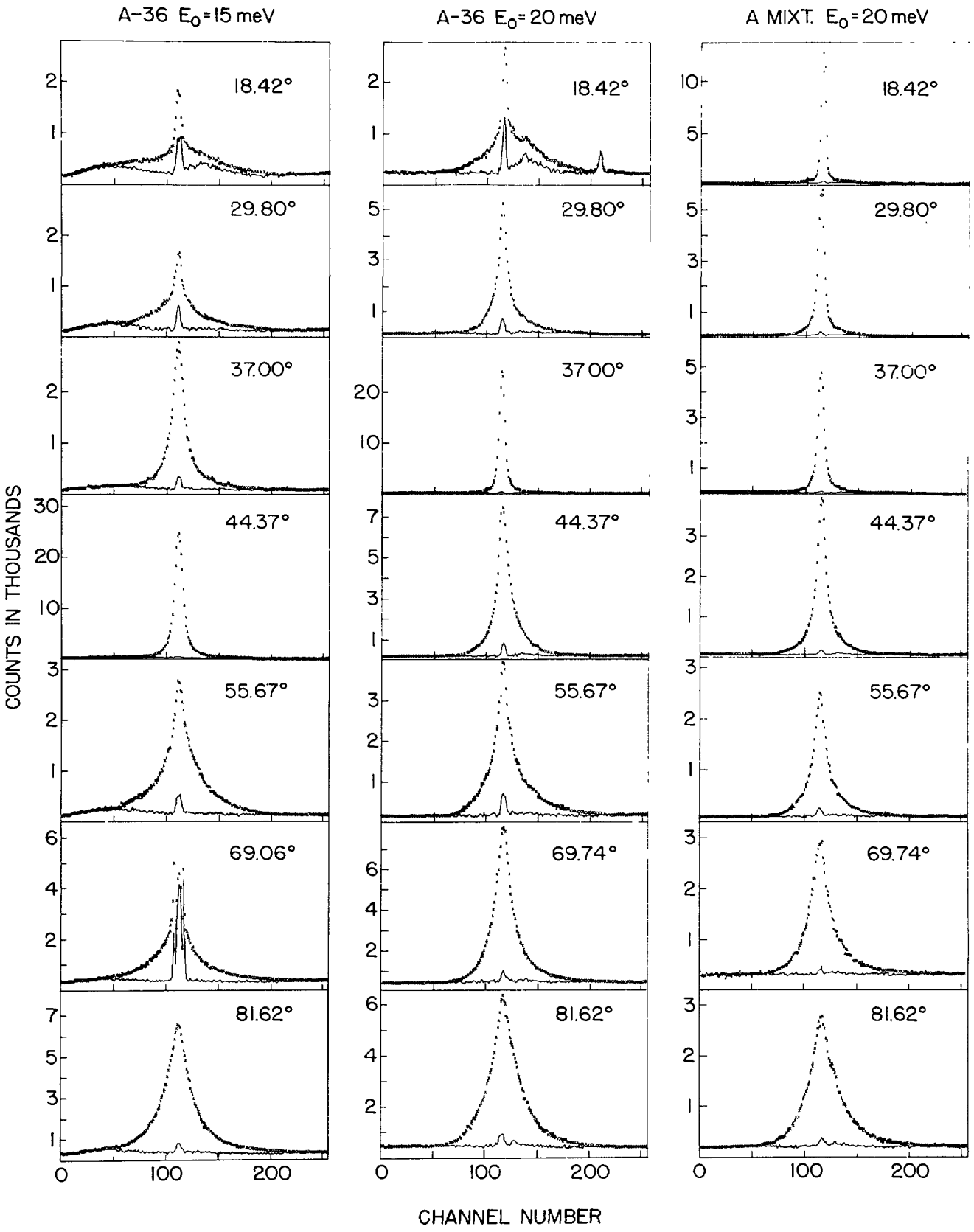
A-36 E_0=15 meV
A-36 E_0=20 meV
A MIXT. E_0=20 meV
18.42°
29.80°
37.00°
44.37°
55.67°
69.06°
69.74°
81.62°
COUNTS IN THOUSANDS
CHANNEL NUMBER
0
100
200

Figure 2

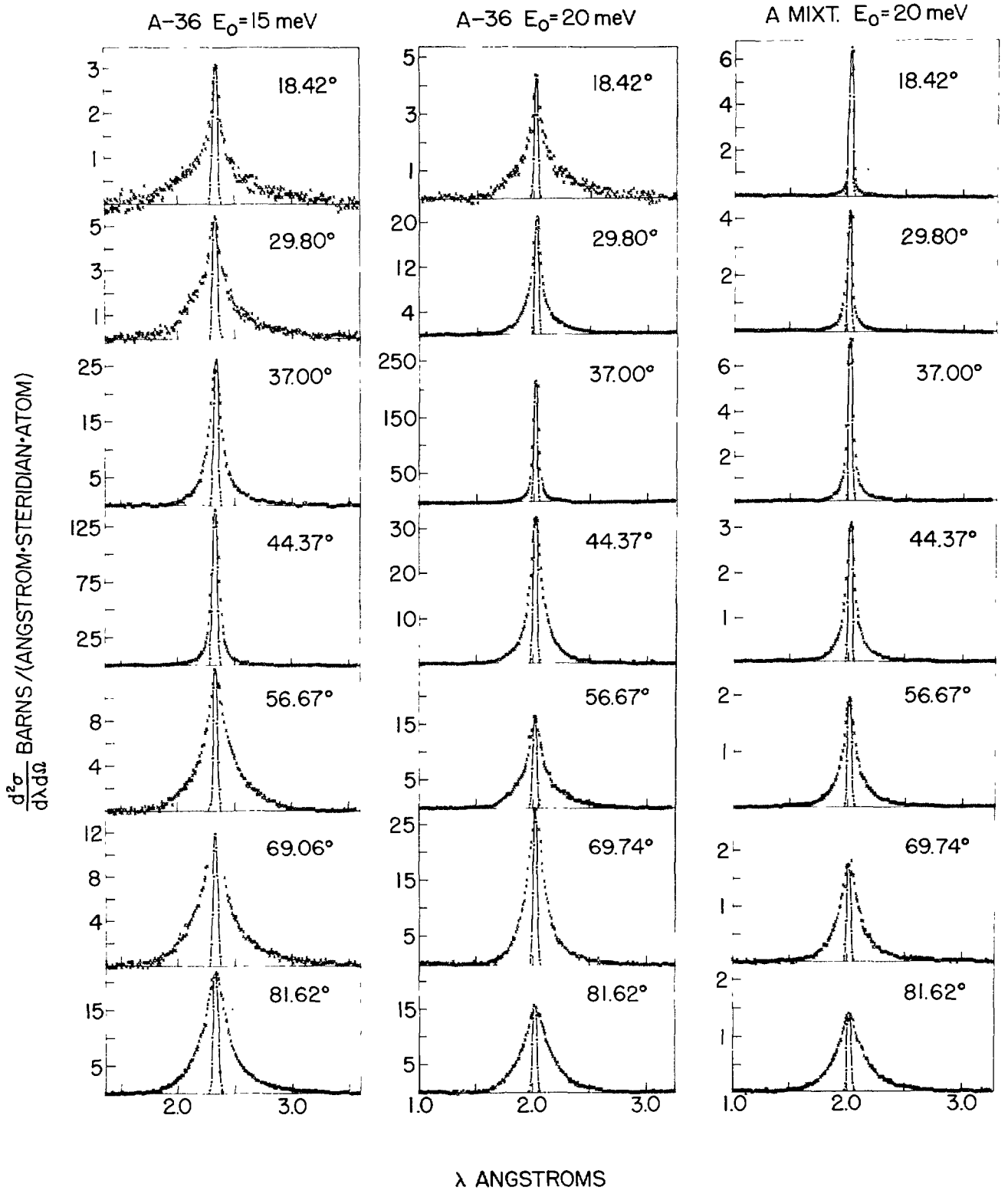
A-36 E_0=15 meV
A-36 E_0=20 meV
A MIXT. E_0=20 meV
18.42°
29.80°
37.00°
44.37°
56.67°
69.06°
69.74°
81.62°
$\frac{d^2\sigma}{d\lambda d\Omega}$ BARNS/(ANGSTROM·STERIDIAN·ATOM)
λ ANGSTROMS

Figure 3

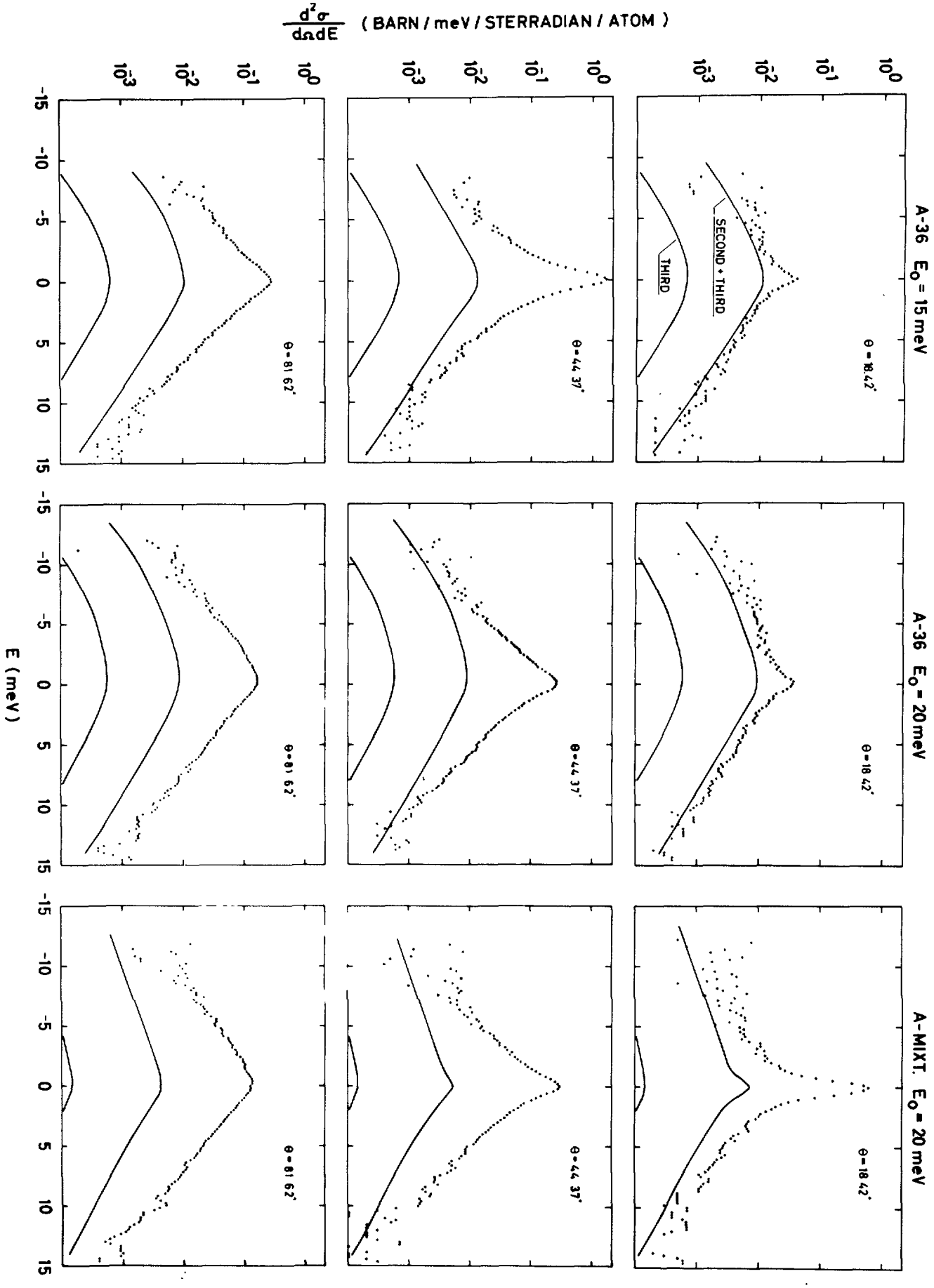
$\frac{d^2\sigma}{d\Omega dE}$ (BARN / meV / STERRADIAN / ATOM)
A-36 E_0 = 15 meV
A-36 E_0 = 20 meV
A-MIXT. E_0 = 20 meV
SECOND + THIRD
THIRD
θ = 18.42°
θ = 44.37°
θ = 81.62°
E (meV)

Figure 4

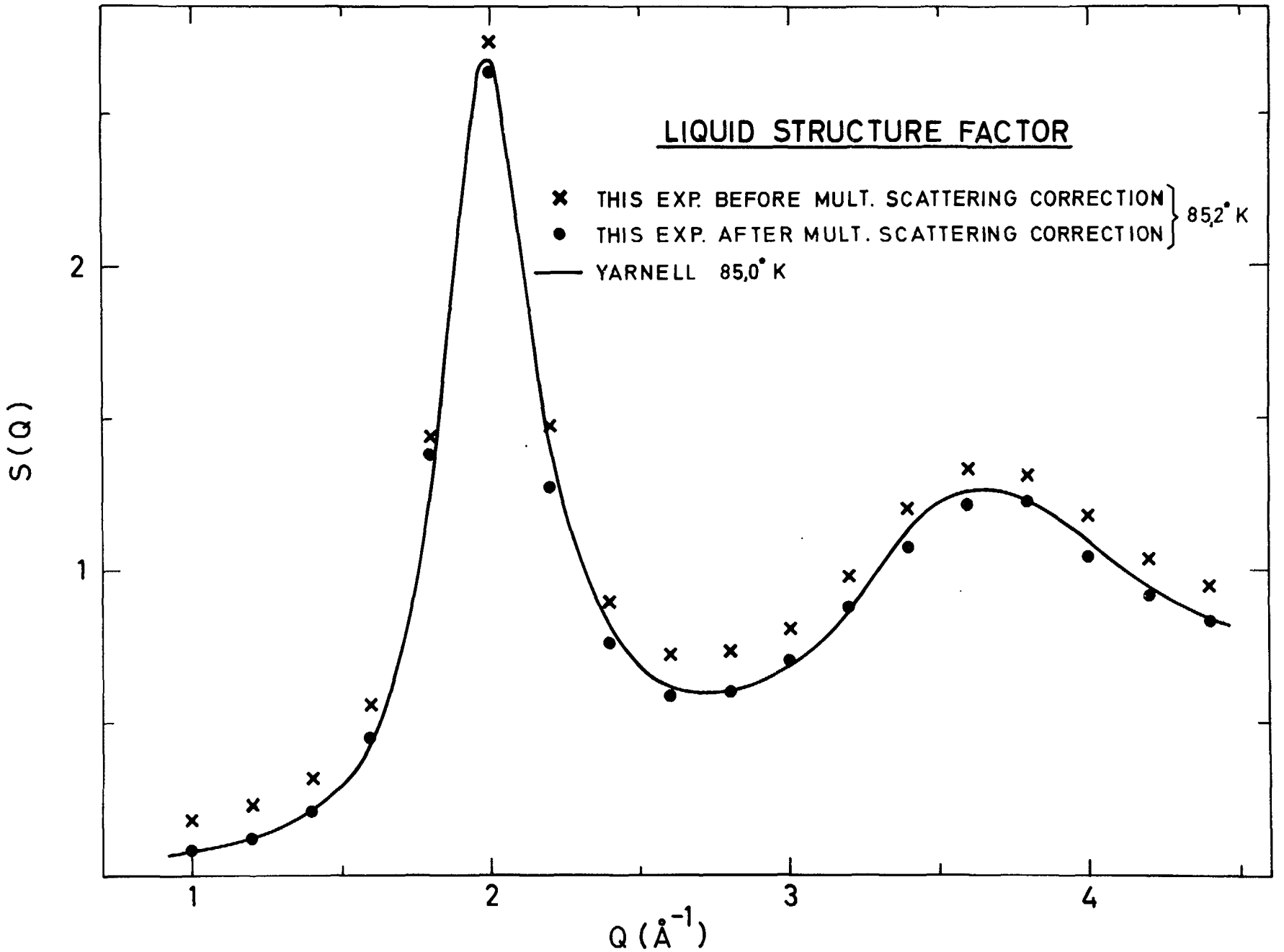
LIQUID STRUCTURE FACTOR
THIS EXP. BEFORE MULT. SCATTERING CORRECTION
THIS EXP. AFTER MULT. SCATTERING CORRECTION
85,2° K
YARNELL 85,0° K
S(Q)
Q (Å^{-1})
1
2
3
4

Figure 5

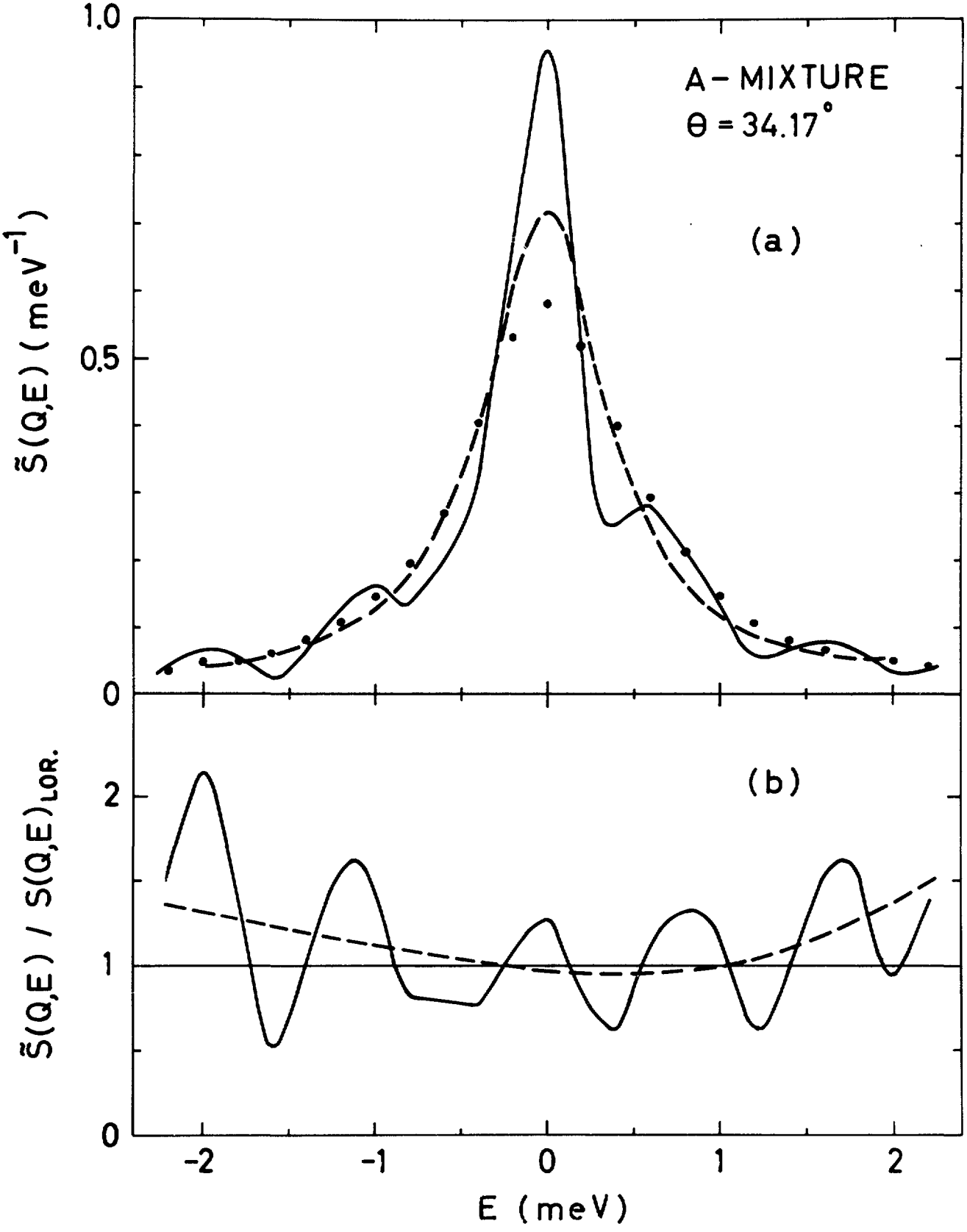

Figure 6

Figure 7

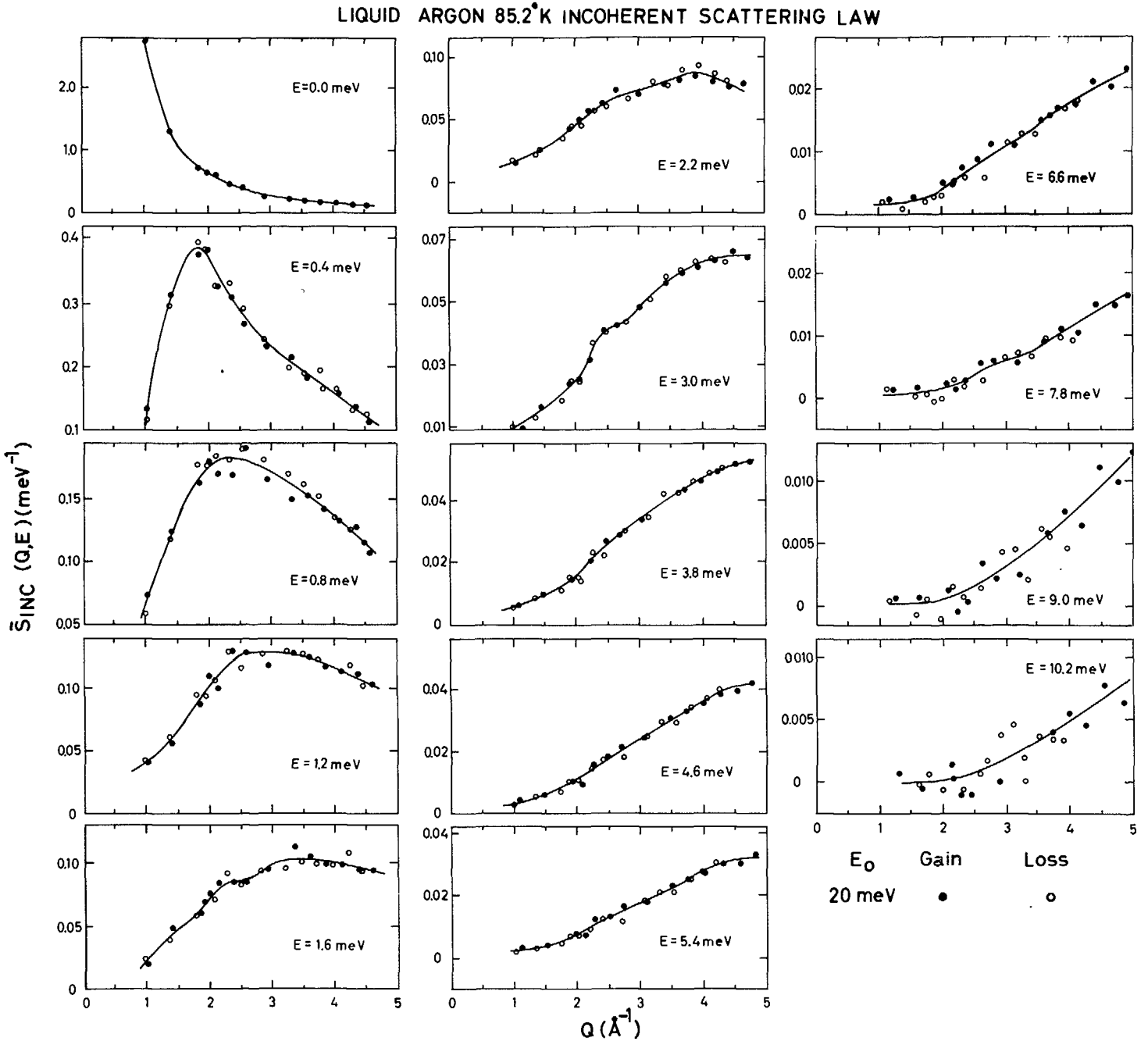
LIQUID ARGON 85.2°K INCOHERENT SCATTERING LAW
E=0.0 meV
E = 2.2 meV
E = 6.6 meV
E=0.4 meV
E = 3.0 meV
E = 7.8 meV
E=0.8 meV
E = 3.8 meV
E = 9.0 meV
E = 1.2 meV
E = 4.6 meV
E = 10.2 meV
E = 1.6 meV
E = 5.4 meV
$\tilde{S}_{INC}$ (Q,E) (meV^{-1})
Q (Å^{-1})
E_o Gain Loss
20 meV

Figure 8

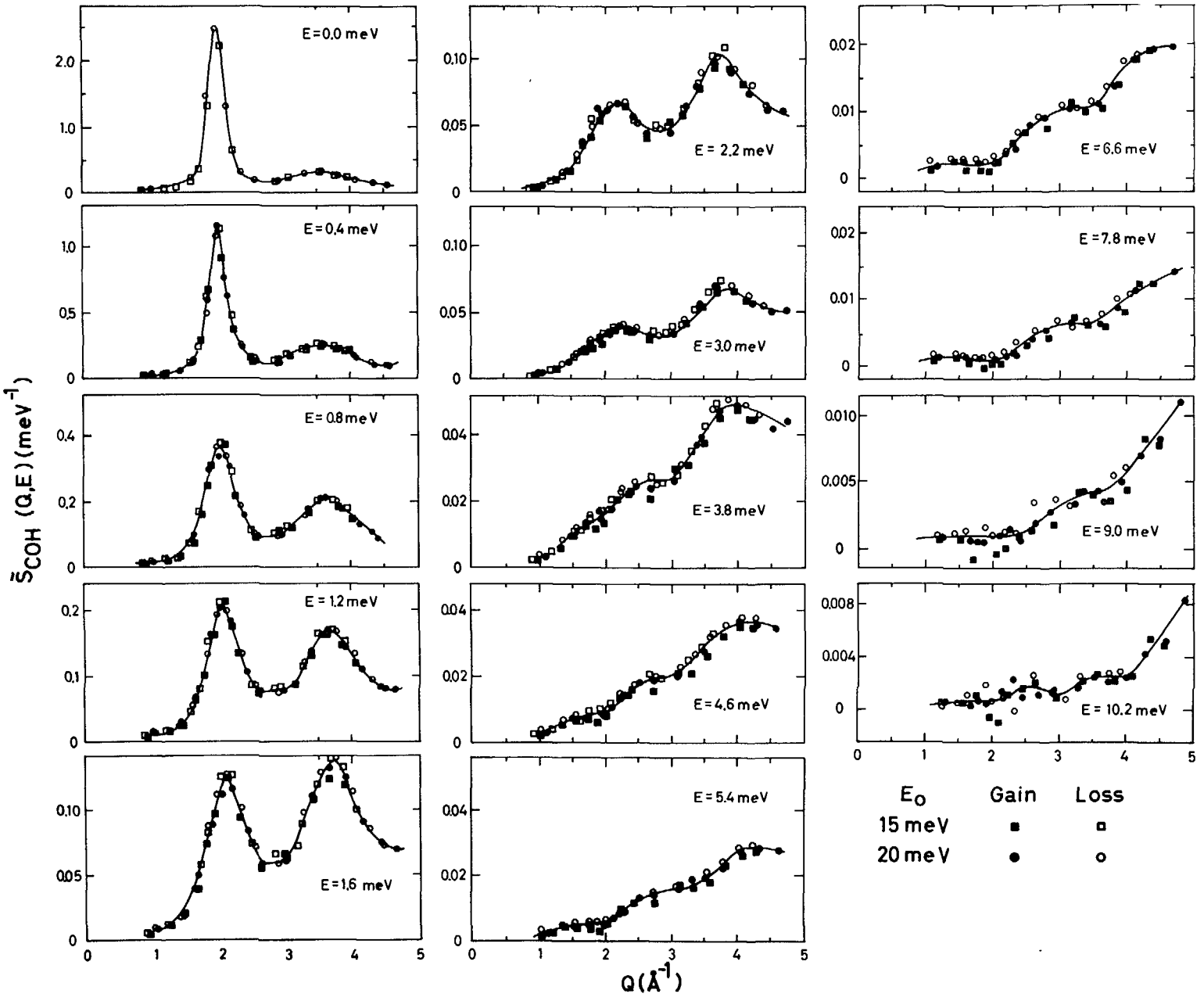
LIQUID ARGON 85.2°K COHERENT SCATTERING LAW
E=0.0 meV
E=0.4 meV
E=0.8 meV
E=1.2 meV
E=1.6 meV
E=2.2 meV
E=3.0 meV
E=3.8 meV
E=4.6 meV
E=5.4 meV
E=6.6 meV
E=7.8 meV
E=9.0 meV
E=10.2 meV
$\tilde{S}_{COH}$ (Q,E) (meV^{-1})
Q(Å^{-1})
E_o Gain Loss
15 meV
20 meV

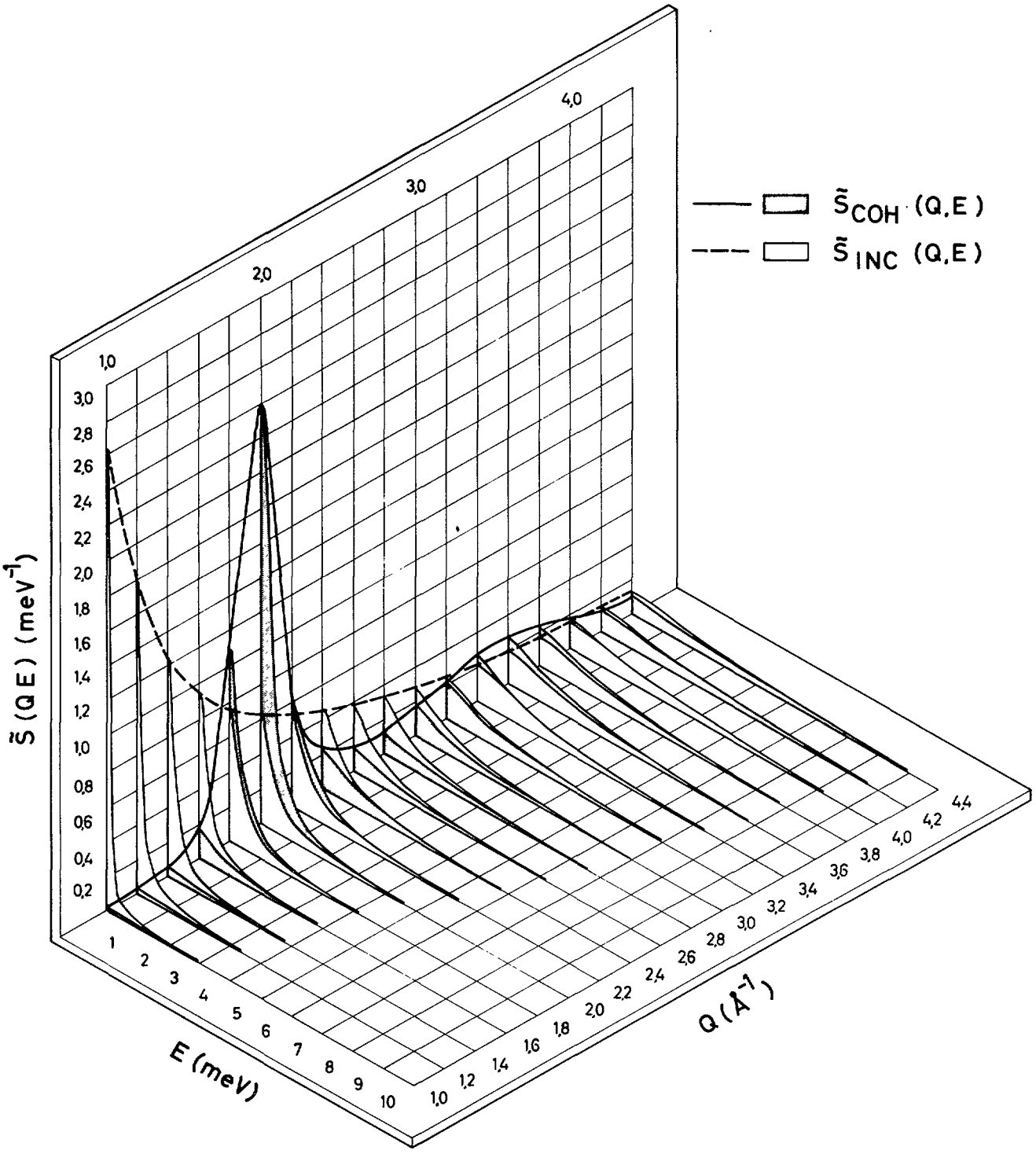

Figure 9

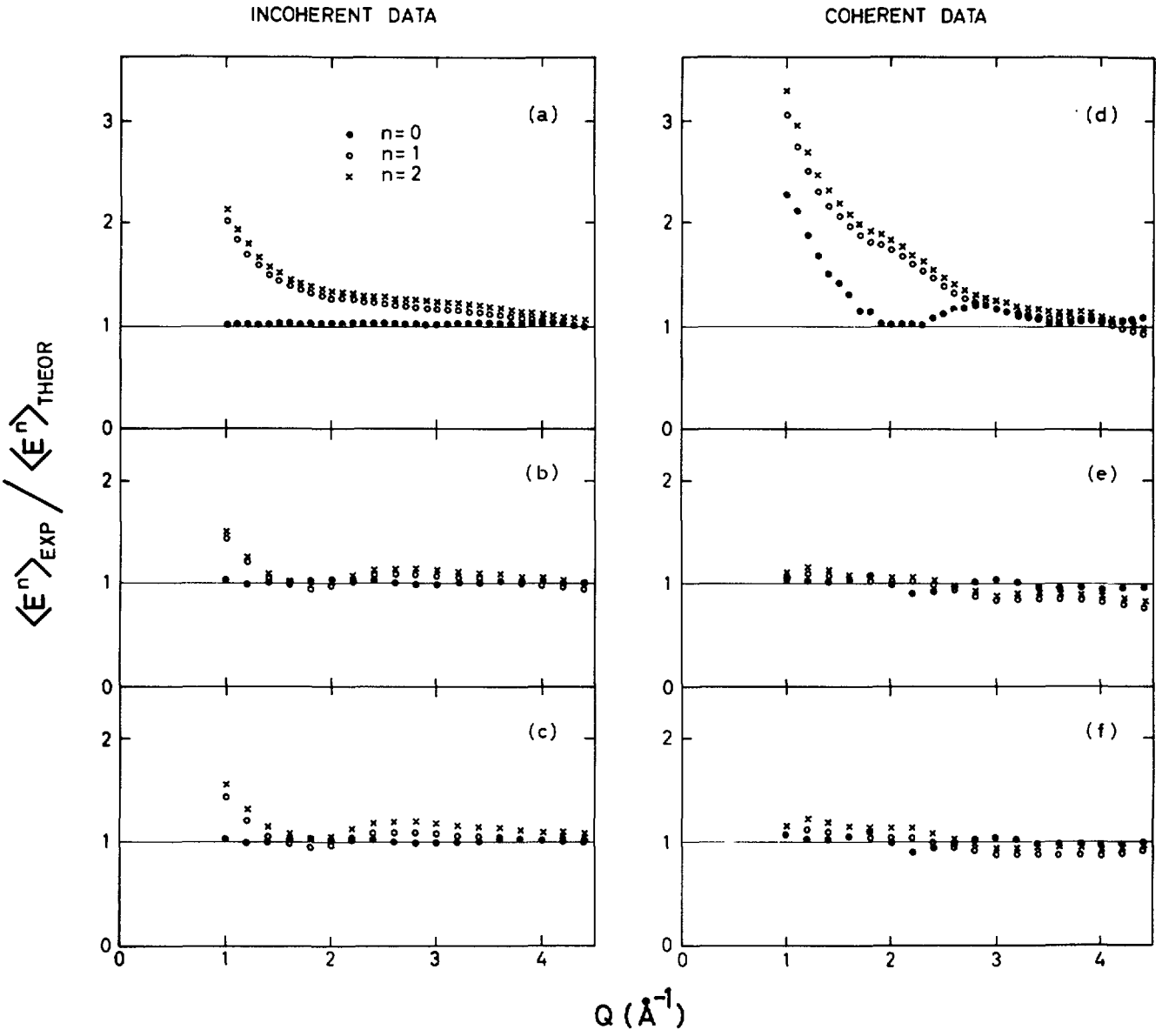
INCOHERENT DATA
COHERENT DATA
(a)
(b)
(c)
(d)
(e)
(f)
n=0
n=1
n=2
$\langle E^n \rangle_{EXP} / \langle E^n \rangle_{THEOR}$
Q (Å^{-1})

Figure 10

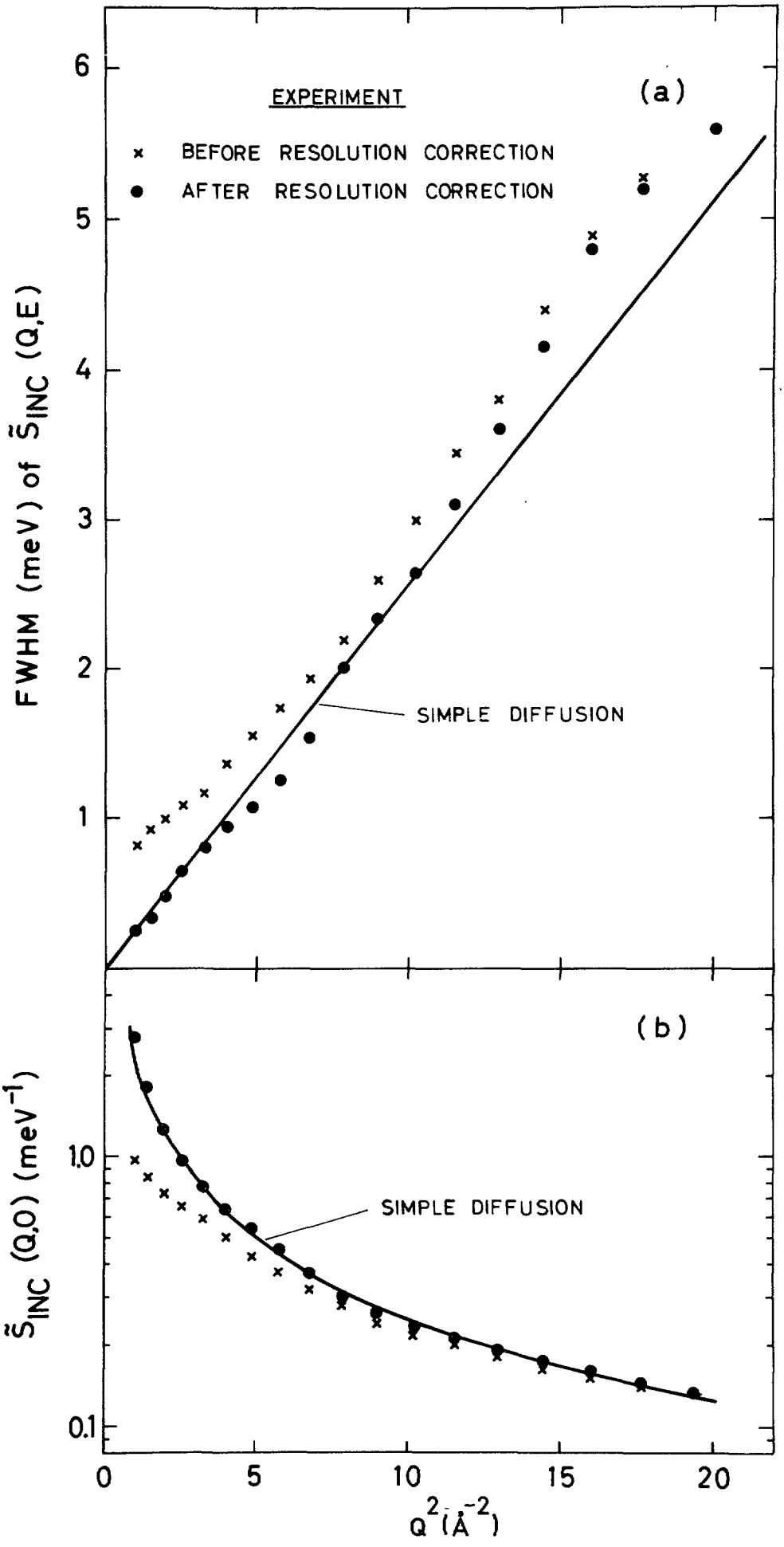
EXPERIMENT
(a)
BEFORE RESOLUTION CORRECTION
AFTER RESOLUTION CORRECTION
SIMPLE DIFFUSION
FWHM (meV) of $\tilde{S}_{INC}$ (Q,E)
(b)
SIMPLE DIFFUSION
$\tilde{S}_{INC}$ (Q,0) (meV^{-1})
Q^2 (Å^{-2})

Figure 11

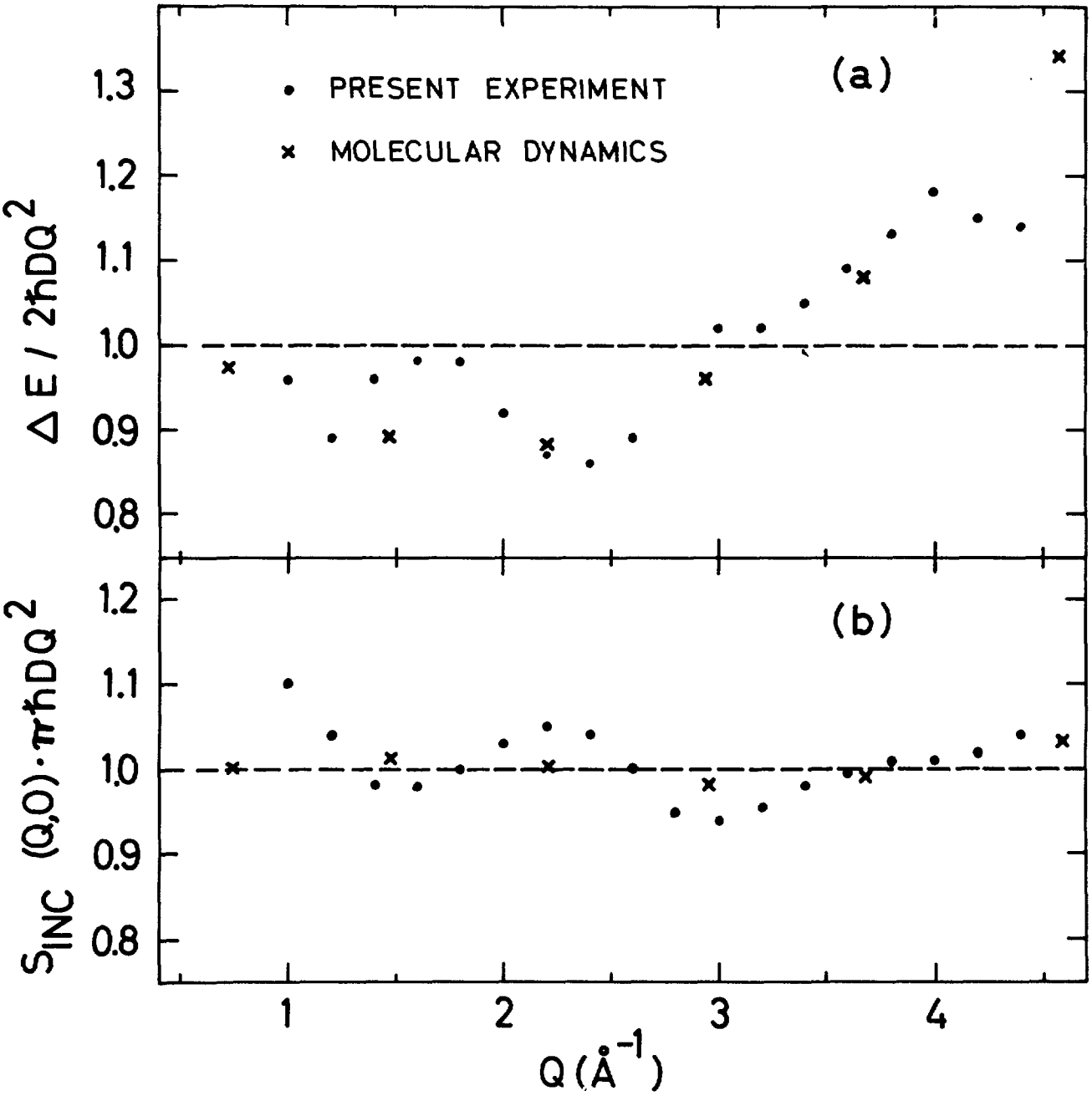
PRESENT EXPERIMENT
MOLECULAR DYNAMICS
(a)
(b)
ΔE / 2ħDQ²
S_INC (Q,0)·πħDQ²
Q (Å⁻¹)
1.3
1.2
1.1
1.0
0.9
0.8
1
2
3
4

Figure 12

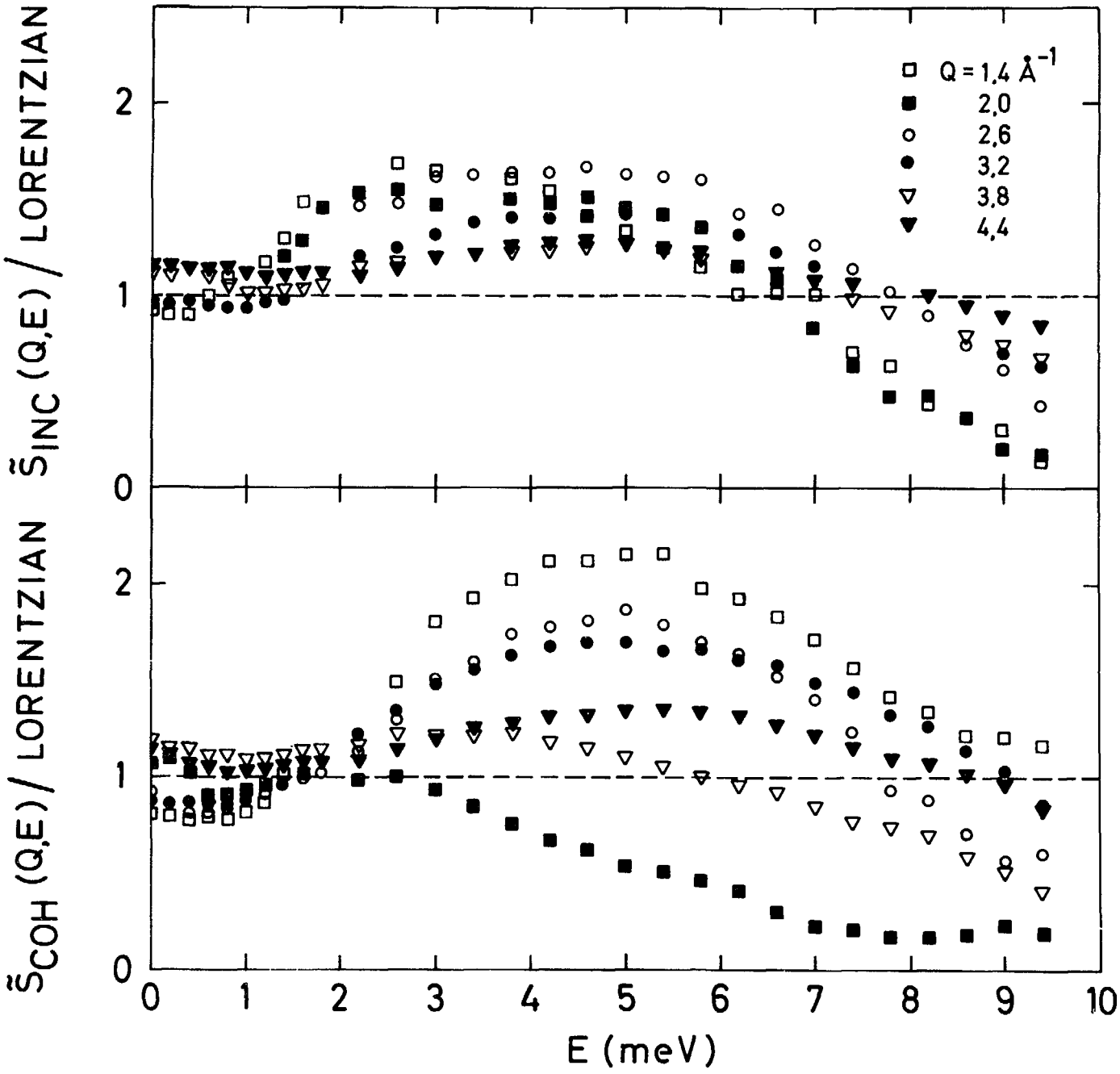
$\tilde{S}_{COH}(Q,E)$ / LORENTZIAN
$\tilde{S}_{INC}(Q,E)$ / LORENTZIAN
Q = 1.4 Å^{-1}
2.0
2.6
3.2
3.8
4.4
0
1
2
0
1
2
3
4
5
6
7
8
9
10
E (meV)

Figure 13

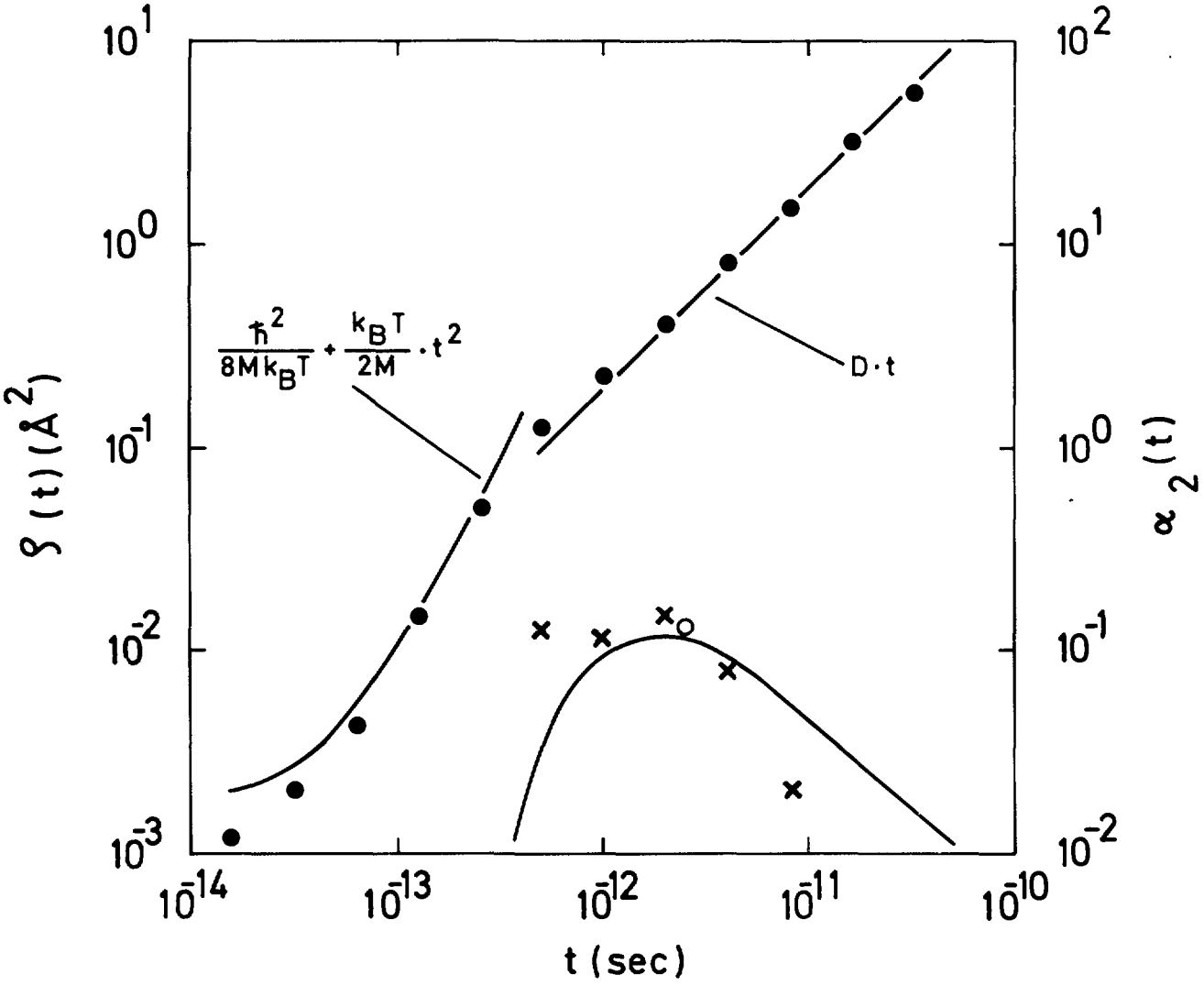
10^1
10^0
10^{-1}
10^{-2}
10^{-3}
10^2
10^1
10^0
10^{-1}
10^{-2}
10^{-14}
10^{-13}
10^{-12}
10^{-11}
10^{-10}
t (sec)
δ (t) (Å^2)
α_2(t)
$\frac{\hbar^2}{8Mk_BT} + \frac{k_BT}{2M} \cdot t^2$
D·t

Figure 14

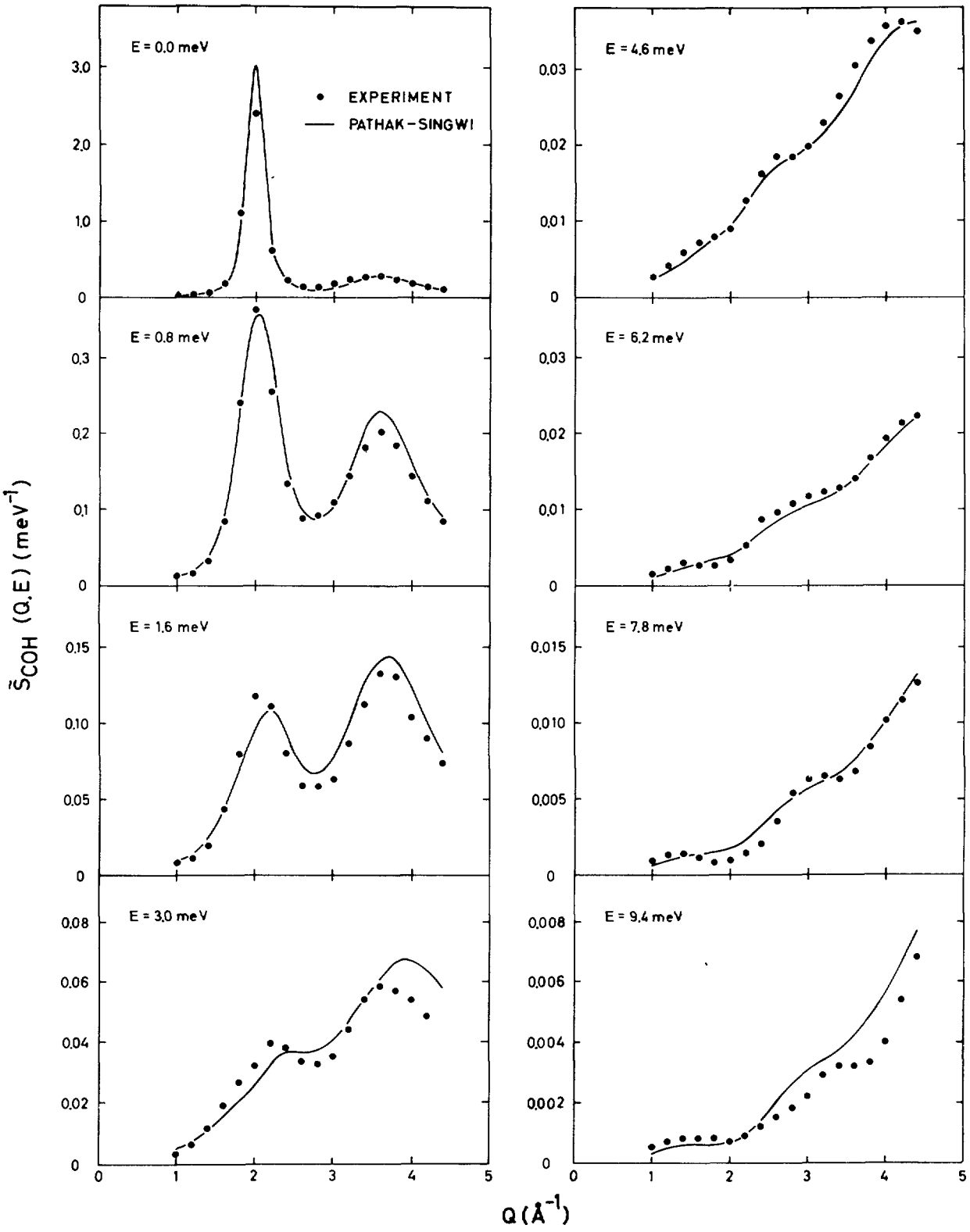
E = 0.0 meV
EXPERIMENT
PATHAK-SINGWI
E = 0.8 meV
E = 1.6 meV
E = 3.0 meV
E = 4.6 meV
E = 6.2 meV
E = 7.8 meV
E = 9.4 meV
$\tilde{S}_{COH}$ (Q,E) (meV^{-1})
Q (Å^{-1})

Figure 15

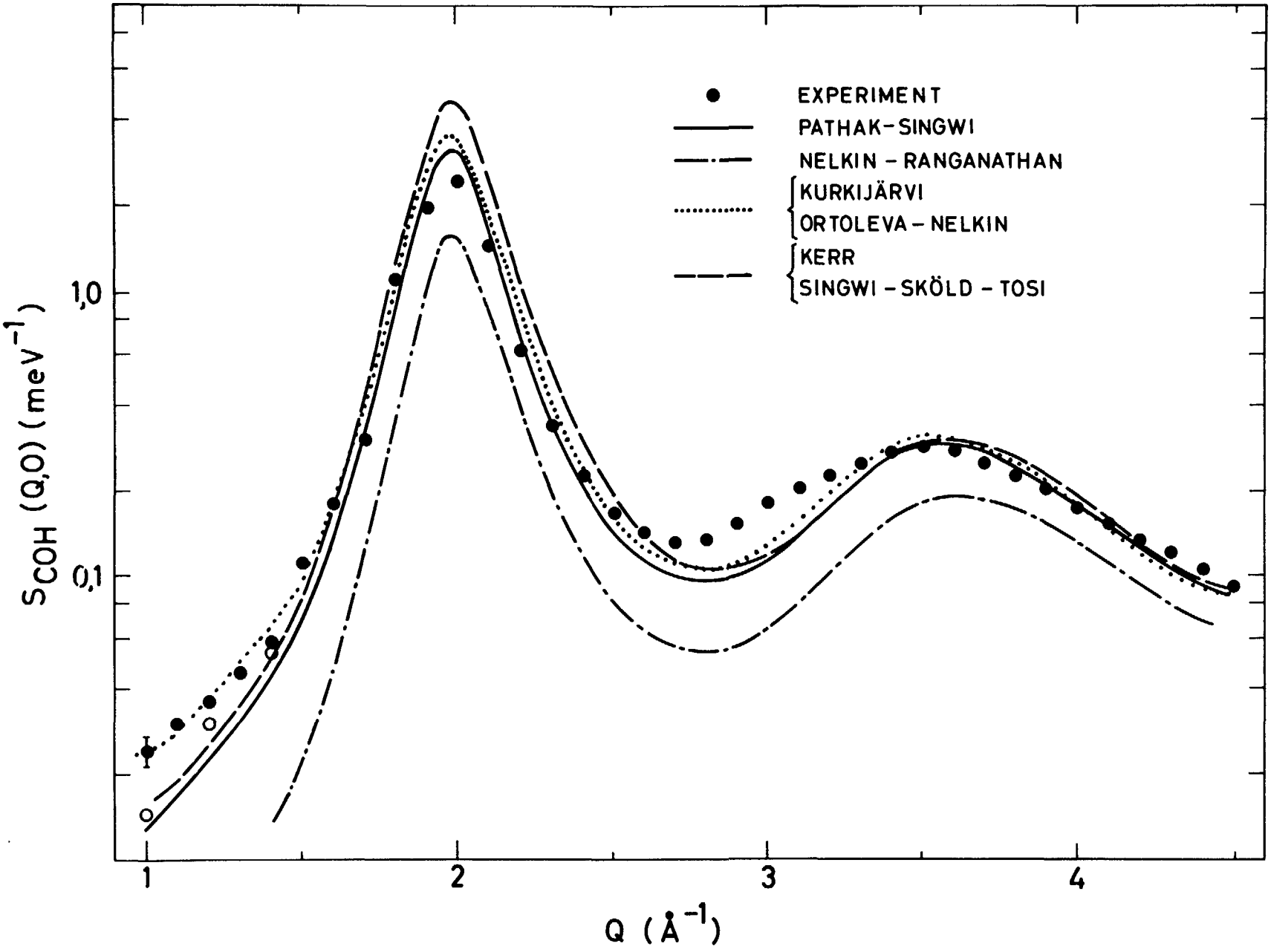
EXPERIMENT
PATHAK-SINGWI
NELKIN - RANGANATHAN
KURKIJÄRVI
ORTOLEVA - NELKIN
KERR
SINGWI - SKÖLD - TOSI
S_{COH} (Q,O) (meV^{-1})
1,0
0,1
1
2
3
4
Q (Å^{-1})

Figure 9

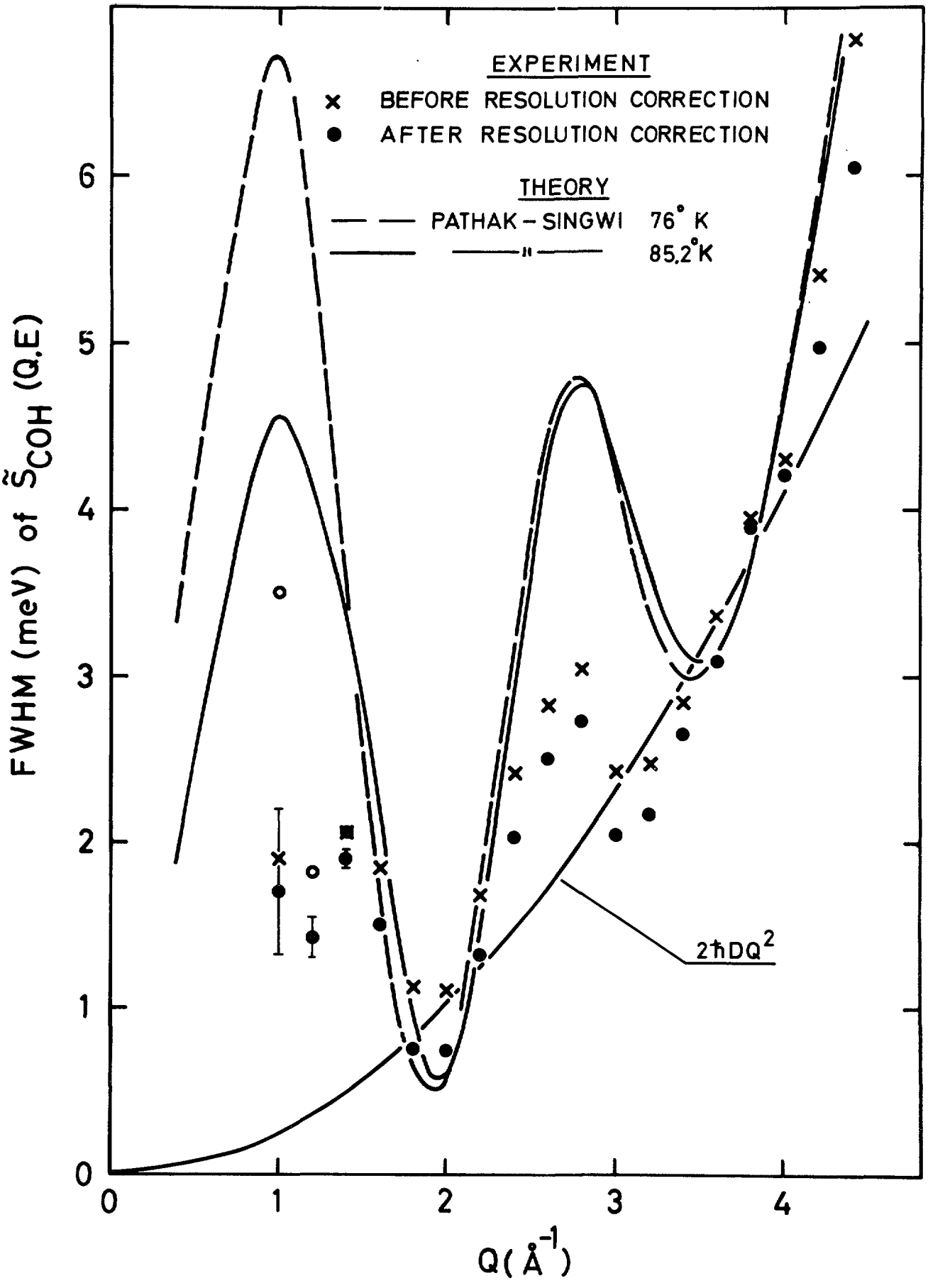
EXPERIMENT
BEFORE RESOLUTION CORRECTION
AFTER RESOLUTION CORRECTION
THEORY
PATHAK – SINGWI 76° K
" 85.2°K
2ħDQ²
FWHM (meV) of S̃COH (Q,E)
Q(Å⁻¹)
0
1
2
3
4
5
6

Figure 17

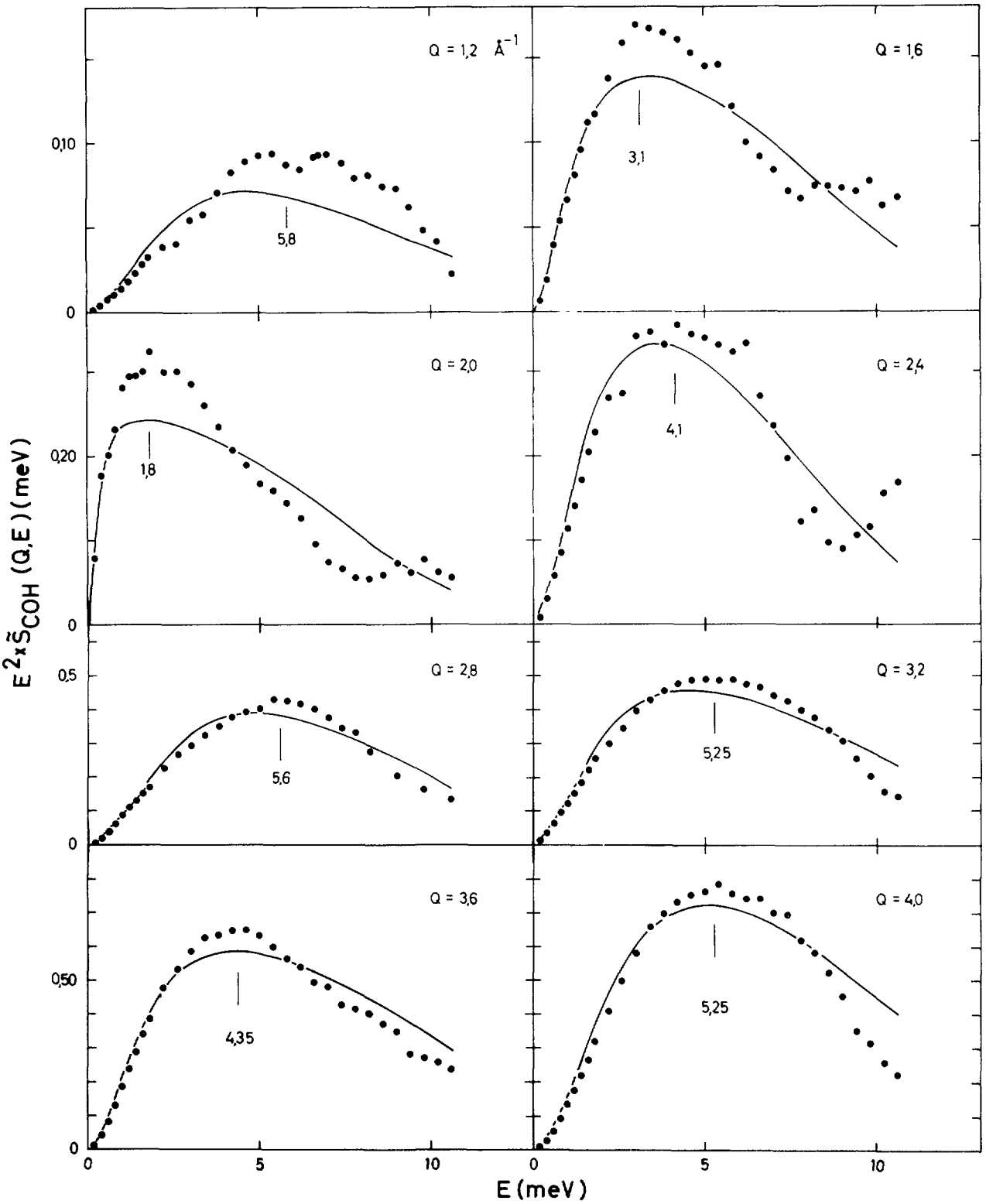
Q = 1,2 Å^{-1}
Q = 1,6
Q = 2,0
Q = 2,4
Q = 2,8
Q = 3,2
Q = 3,6
Q = 4,0
5,8
3,1
1,8
4,1
5,6
5,25
4,35
5,25
0,10
0,20
0,5
0,50
0
5
10
E (meV)
$E^2 x \tilde{S}_{COH}(Q,E)$ (meV)

Figure 18

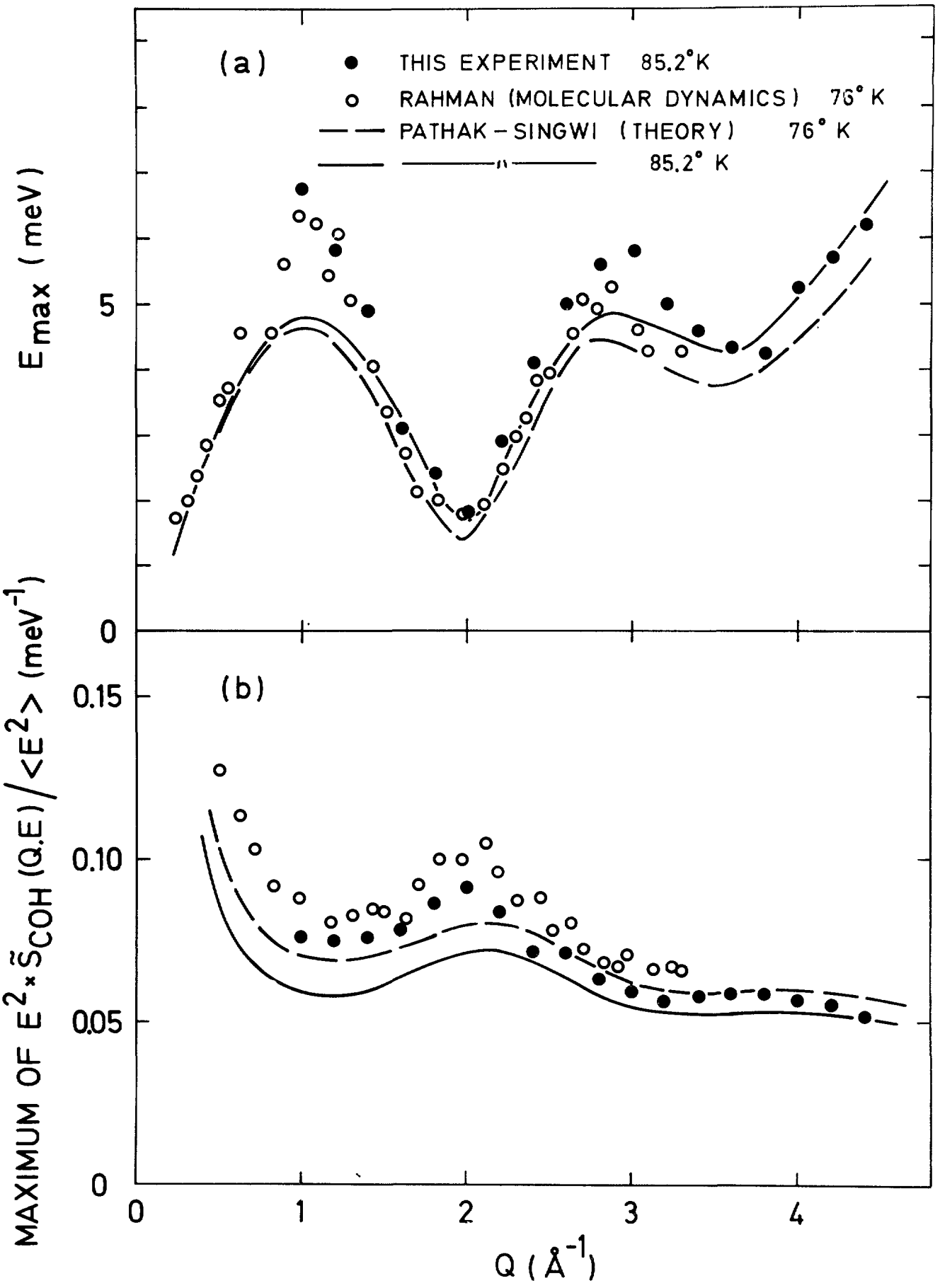
(a)
THIS EXPERIMENT 85.2°K
RAHMAN (MOLECULAR DYNAMICS) 76° K
PATHAK – SINGWI (THEORY) 76° K
85.2° K
E_{max} (meV)
5
0
(b)
MAXIMUM OF $E^2 \times \tilde{S}_{COH}(Q,E) / \langle E^2 \rangle$ (meV^{-1})
0.15
0.10
0.05
0
0
1
2
3
4
Q (Å^{-1})

Figure 19

LIST OF PUBLISHED AE-REPORTS

1–370 (See back cover earlier reports.)

371. Transition probabilities in the 1/2+(631) Band in ^{235}U. By M. Höjeberg and S. G. Malmskog 1969. 18 p. Sw. cr. 10:–.
372. E2 and M1 transition probabilities in odd mass Hg nuclei. By V. Berg, A Bäcklin, B Fogelberg and S. G. Malmskog. 1969. 19 p. Sw. cr. 10:–
373. An experimental study of the accuracy of compensation in lithium drifted germanium detectors. By A. Lauber and B. Malmsten. 1969. 25 p. Sw cr 10:–.
374. Gamma radiation from fission fragments. By J. Higbie. 1969. 22 p. Sw. cr. 10:–
375. Fast neutron elastic and inelastic scattering of vanadium. By B Holmqvist, S. G. Johansson, G. Lodin and T. Wiedling. 1969. 48 p. Sw. cr. 10:–
376. Experimental and theoretical dynamic study of the Agesta nucler power station. By P Å. Bliselius, H. Vollmer and F. Åkerhielm. 1969. 39 p Sw. cr. 10:–.
377. Studies of Redox equilibria at elevated temperatures 1. The estimation of equilibrium constants and standard potentials for aqueous systems up to 374°C. By D. Lewis. 1969. 47 p. Sw. cr. 10:–.
378 The whole body monitor HUGO II at Studsvik. Design and operation By L Devell, I. Nilsson and L. Venner. 1970. 26 p. Sw cr. 10:–
279. ATOMSPHERIC DIFFUSION. Investigations at Studsvik and Agesta 1960–1963. By L-E. *Hæggblom, Ch. Gyllander and U. Widemo 1969 91 p* Sw cr 10:–
380. An expansion method to unfold proton recoil spectra. By J. Kockum. 1970. 20 p. Sw. cr. 10:–.
381. The 93.54 keV lever ^{91}Sr, and evidence for 3-neutron states above N=50. By S G. Malmskog and J. McDonald 1970. 24 p. Sw. cr. 10:–.
382. The low energy level structure of ^{191}Ir. By S. G. Malmskog, V. Berg, A. Bäcklin and G Hedin. 1970. 24 p Sw cr 10:–.
383. The drinking rate of fish in the Skagerack and the Baltic. By J. E. Larsson. 1970. 16 p. Sw. cr. 10:–.
384. Lattice dynamics of Nacl, KCl, RbCl and RbF. By G. Raunio and S. Rolandson. 1970. 26 p. Sw. cr. 10:–.
385. A neutron elastic scattering study of chromium, iron and nickel in the energy region 1.77 to 2.76 MeV. By B. Holmqvist, S. G. Johansson, G. Lodin, M Salama and T. Wiedling. 1970. 26 p. Sw. cr. 10:–.
386. The decay of bound isobaric analogue states in ^{28}Si and ^{32}Si using (d. nγ) reactions. By L. Nilsson, A Nilsson and I. Bergqvist. 1970. 34 p. Sw. cr. 10–.
387. Transition probabilities in ^{189}Os. By S G. Malmskog, V. Berg and A. Bäck*lin. 1970 40 p. Sw. cr. 10:–.*
388. Cross sections for high-energy gamma transition from MeV neutron capture in ^{208}Pb. By I. Bergqvist, B. Lundberg and L. Nilsson. 1970. 16 p. Sw. cr. 10:–.
389. High-speed, automatic radiochemical separations for activation analysis in the biological and medical research laboratory. By K. Samsahl. 1970. 18 p. Sw. cr. 10:–.
390. Use of fission product Ru-106 gamma activity as a method for estimating the relative number of fission events in U-235 and Pu-239 in low-enriched fuel elements. By R. S. Forsyth and W. H. Blackadder. 1970. 26 p. Sw. cr. 10:–.
391. Half-life measurements in ^{134}I. By V. Berg and A. Höglund. 1970. 16 p Sw. cr. 10:–.
392. Measurement of the neutron spectra in FRO cores 5, 9 and PuB-5 using resonance sandwich detectors. By T. L. Andersson and M. N. Qazi. 1970. 30 p. Sw. cr. 10:–.
393. A gamma scanner using a Ge(Li) semi-conductor detector with the possibility of operation in anti-coincidence mode. By R. S. Forsyth and W. H. Blackadder. 1970. 22 p. Sw. cr. 10:–.
394. A study of the 190 keV transition in ^{141}La. By B. Berg, A. Höglund and B. *Fogelberg. 1970 22 p. Sw cr. 10:–.*
395. Magnetoacoustic waves and instabilities in a Hall-effect-dominiated plasma. By S. Palmgren. 1970. 20 p. Sw. cr. 10:–.
396. A new boron analysis method. By J. Weitman, N. *Dåverhög* and S. *Farvol*den. 1970. 26 p. Sw. cr. 10:–.
397. Progress report 1969. Nuclear chemistry. 1970. 39 p. Sw. cr. 10:–.
398. Prompt gamma radiation from fragments in the thermal fission of ^{235}U. By H. Albinsson and L. Lindow. 1970. 48 p. Sw. cr. 10:–.
399. Analysis of pulsed source experiments performed in copper-reflected fast assemblies. By J. Kockum. 1970. 32 p. Sw. cr. 10:–.
400. Table of half-lives for excited nuclear levels. By S. G. Malmskog. 1970. 33 p. Sw. cr. 10:–.
401. Needle type solid state detectors for in vivo measurement of tracer activity. By A. Lauber, M. Wolgast. 1970. 43 p. Sw. cr. 10:–.
402. Application of pseudo-random signals to the Agesta nuclear power station By P-Å. Bliselius. 1970. 30 p. Sw. cr. 10:–.
403. *Studies of redox equilibria at elevated temperatures 2. An automatic di*vided-function autoclave and cell with flowing liquid junction for electrochemical measurements on aqueous systems. By. K. Johnsson, D. Lewis and *M. de Pourbaix. 1970. 38 p. Sw. cr. 10:–.*
404. Reduction of noise in closed loop servo systems. By K. Nygaard. 1970. 23 p. Sw. cr. 10:–.
405. Spectral parameters in water-moderated lattices. A survey of experimental *data with the aid of two-group formulae.* By E. K. Sokolowski. 1970. 22 p. Sw. cr. 10:–.
406. The decay of optically thick helium plasmas, taking into account ionizing collisions between metastable atoms or molecules. By J. Stevefelt. 1970. 18 p. Sw. cr. 10:–.
407. Zooplankton from Lake Magelungen, Central Sweden 1960-63. By E. Almquist. 1970. 62 p. Sw. cr. 10:–.
408. A method for calculating the washout of elemental iodine by water sprays. By E Bachofner and R. Hesböl. 1970. 24 p. Sw. cr. 10:–.
409. X-ray powder diffraction with Guinier–Hägg focusing cameras. By A. Brown. 1970. 102 p. Sw. cr 10:–.
410. General physic section Progress report. Fiscal year 1969/70. By J. Braun. 1970. 92 p. Sw. cr. 10:–.
411. In-pile determination of the thermal conductivity of UO_2 in the range 500–2 500 degrees centigrade. By J-Å Gyllander. 1971. 70 p. Sw. cr. 10:–.
412. A study of the ring test for *determination of transverse ductility of fuel* element canning. By G. Anevi and G. Östberg. 1971. 17 p. Sw. cr. 15:–.
413. Pulse radiolysis of Aqueous Solutions of aniline and substituted anilines. By H. C. Christensen. 1971. 40 p. Sw. cr. 15:–.
414. Radiolysis of aqueous toluene solutions. By H. C. Christensen and R. Gustafson. 1971. 20 p. Sw. cr. 15:–.
415. The influence of powder characteristics on process and product parameters in UO_2 pelletization. By U. Runfors. 1971. 32 p. Sw. cr. 15:–.
416. Quantitative assay of Pu239 and Pu240 by neutron transmission measurements. By E. Johansson. 1971. 26 p. Sw. cr 15:–.
417. Yield of prompt gamma radiation in slow-neutron induced fission of ^{235}U as a function of the total fragment kinetic energy. By H. Albinsson. 1971. 38 p. Sw. cr. 15:–.
418. Measurements of the spectral light emission from decaying high pressure helium plasmas. By J. Stevefelt and J. Johansson. 1971. 48 p. Sw. cr. 15:–.
419. Progress report 1970. Nuclear chemistry. 1971. 32 p. Sw. cr. 15:–.
420. Energies and yields of prompt gamma rays from fragments in slow-neutron induced fission of ^{235}U. By H. Albinsson. 1971. 56 p. Sw. cr. 15:–.
421. Decay curves and half-lives of gamma-emitting states from a study of prompt fission gamma radiation. By H. Albinsson. 1971. 28 p. Sw. cr. 15:–.
422. Adjustment of neutron cross section data by a least square fit of calculated quantities to experimental results. Part 1. Theory. By H. Häggblom. 1971. 28 p. Sw. cr. 15:–.
423. Personnel dosimetry at AB Atomenergi during 1969. By J. Carlsson and T. Wahlberg. 1971. 10 p. Sw. cr. 15:–.
424. Some elements of equilibrium diagrams for systems of iron with water above 100°C and with simple chloride, carbonate and sulfate melts. By D. Lewis. 1971. 40 p. Sw. cr. 15:–.
425. A study of material buckling in uranium-loaded assemblies of the fast reactor FR0. By R. Håkansson and L. I. Tirén. 1971. 32 p. Sw. cr. 15:–.
426. Dislocation line tensions in the noble metals, the alkali metals and β-Brass. By B. Pettersson and K. Malén. 1971. 14 p. Sw. cr. 15:–.
427. Studies of fine structure in the flux distribution due to the heterogeneity in some FR0 cores. By T. L. Andersson and H. Häggblom. 1971. 32 p. Sw. cr. 15:–.
428. Integral measurement of fission-product reactivity worths in some fast reactor spectra. By T. L. Andersson. 1971. 36 p. Sw. cr. 15:–.
429. Neutron energy spectra from neutron induced fission of ^{235}U at 0.95 MeV and of ^{238}U at 1.35 and 2.02 MeV. By E. Almén, B. Holmqvist and T. Wiedling. 1971. 16 p. Sw. cr. 15:–.
430. Optical model analyses of experimental fast neutron elastic scattering data. By B. Holmqvist and T. Wiedling. 1971. 238 p. Sw. cr. 20:–.
431. Theoretical studies of aqueous systems above 25°C. 1. Fundamental concepts for equilibrium diagrams and some general features of the water system. By Derek Lewis. 1971. 27 p. Sw. cr. 15:–.
432. Theoretical studies of aqueous systems above 25°C . 2. The iron – water system. By Derek Lewis. 1971. 41 p. Sw. cr. 15:–.
433. A detector for (n,γ) cross section measurements. *By J Hellström* and S. Beshai. 1971. 22 p. Sw. cr. 15:–.
434. Influence of elastic anisotropy on extended dislocation nodes. By B. Pettersson. 1971. 27 p. Sw. cr. 15:–.
435. Lattice dynamics of CsBr. By S. Rolandson and G. Raunio. 1971. 24 p. Sw. cr. 15:–.
436. The hydrolysis of iron (III) and iron (II) ions between 25°C and 375°C. By Derek Lewis. 1971.16 p. Sw. cr. 15:–.
437. Studies of the tendency of intergranular corrosion cracking of austenitic Fe-Cr-Ni alloys in high purity water at 300°C. By W. Hübner, B. Johansson and M. de Pourbaix. 1971. 30 p. Sw. cr. 15:–.
438. Studies concerning water-surface deposits in recovery boilers. By O. Strandberg, J. Arvesen and L. Dahl. 1971. 132 p. Sw. cr. 15:–.
439. Adjustment of neutron cross section data by a least square fit of calculated quantities to experimental results. Part II. Numerical results. By H. Häggblom. 1971. 70 p. Sw. cr. 15:–.
440. Self-powered neutron and gamma detectors for in-core measurements. By O. Strindehag. 1971. 16 p. Sw. cr. 15:–.
441. Neutron capture gamma ray cross sections for Ta, Ag, In and Au between *30 and 175 keV. By J. Hellström and S. Beshai. 1971. 30 p. Sw. cr. 15:–.*
442. Thermodynamical properties of the solidified rare gases. By I. Ebbsjö. 1971. 46 p. Sw. cr. 15:–.
443. Fast neutron radiative capture cross sections for some important standards from 30 keV to 1.5 MeV. By J. Hellström. 1971. 22 p. Sw. cr. 15:–.
444. A Ge (Li) bore hole probe for in situ gamma ray spectrometry. By A. Lauber and O. Landström. 1971. 26 p. Sw. cr. 15:–.
445. Neutron inelastic scattering study of liquid argon. By K. Sköld, J. M. Rowe, G. Ostrowski and P. D. Randolph. 1972. 62 p. Sw. cr. 15:–.

List of published AES-reports (In Swedish)

1. Analysis by means of gamma spectrometry. By D. Brune. 1961. 10 p. Sw. cr. 6:–.
2. Irradiation changes and neutron atmosphere in reactor pressure vessels-some points of view. By M. Grounes. 1962. 33 p. Sw. cr. 6:–.
3. Study of the elongation limit in mild steel. By G. Östberg and R. Attermo. 1963. 17 p. Sw. cr. 6:–.
4. Technical purchasing in the reactor field. By Erik Jonson. 1963. 64 p. Sw. cr. 8:–.
5. Agesta nuclear power station. Summary of technical data, descriptions, etc. for the reactor. By B. Lilliehöök. 1964. 336 p. Sw. cr. 15:–.
6. Atom Day 1965. Summary of lectures and discussions. By S. Sandström. 1966. 321 p. Sw. cr. 15:–.
7. Building materials containing radium considered from the radiation protection point of view. By Stig O. W. Bergström and Tor Wahlberg. 1967. 26 p. Sw. cr. 10:–.
8. Uranium market. 1971. 30 p. Sw. cr. 15:–.
9. Radiography day at Studsvik. Tuesday 27 april 1971. Arranged by AB Atomenergi, IVA's Committee for nondestructive testing and TRC AB. 1971. 102 p. Sw. cr. 15:–.

Additional copies available from the Library of AB Atomenergi, Fack, S-611 01 Nyköping 1, Sweden.

EOS-tryckerierna, Stockholm 1971